VOLUMETRIC CURVATURE AND COHERENCY ASSISTED FAULT MAPPING AND FRACTURE PREDICTION OF CARBONATE RESERVOIR HUABEI FIELD, NORTH CHINA

A Thesis

by

ALLEN XIN LI

Submitted to the Office of Graduate and Professional Studies of
Texas A&M University
in partial fulfillment of the requirements for the degree of

MASTER OF SCIENCE

Chair of Committee,	Yuefeng Sun
Committee Members,	Mark E. Everett
	Zoya Heidari
Head of Department,	Rick Giardino

August 2014

Major Subject: Geophysics

ABSTRACT

Seismic attribute analysis in recent decades has been an instrumental tool in improving the quality of reservoir characterization for hydrocarbon identification. Coherency and curvature are geometric seismic attributes which measure seismic continuity and are particularly useful in mapping the structure and shape of geological features of interest, such as faults, channels and fractures. As these geologic features are prevalent in carbonate fields and heavily influence the productivity of reservoirs in these fields, accurate fault/fracture description employing coherence and curvature analysis is advantageous from a prospecting and production standpoint. It is these attributes that are most useful in fault and fracture characterization in carbonates, and are thus the focus of my investigation.

With a 3D dataset and well data from the Huabei Field in North China, a carbonate reservoir is identified and interpreted through the field. We use the reservoir top depth to narrow our window of investigation of coherence and curvature values through the dataset. Cross-correlation, variance, and eigenstructure-driven coherence as well as volumetric curvature are calculated through the dataset in order to map the regional and small-scale faulting.

Results show that eigenstructure-based coherence analysis generally produces the best general fault analysis for our data, which is attributed to the eigenstructure calculation's separation of waveform and amplitude into mathematically independent measures which are evaluated separately and then analyzed together.

Analyzing the results of cross-correlation, variance/ant-tracking, and eigenstructure-coherence, we are able to observe general faulting and channel behavior, as well as some

smaller-scale fault detail when the data volumes are preconditioned with dip-estimates. Used together with volumetric curvature analysis, which identifies small faults and possible fractures in greater detail, we are able to identify the areas in our reservoir with smaller faults and thus highest probability of fractures, which are strong hydrocarbon indicators in carbonates.

This study demonstrates the capacity of seismic coherence and curvature to delineate faults and fractures in complex carbonate fields, enhances our understanding of how to apply the optimal coherence/curvature methods and their respective parameters to identify different geologic features, and enables us to apply these attribute analysis findings towards prospect identification and production planning in carbonate fields.

ACKNOWLEDGEMENTS

I would like to thank my committee chair, Dr. Sun, and my committee members, Dr. Mark Everett and Dr. Zoya Heidari, for their guidance and support through the course of my studies, research, and development as a geoscientist.

Thanks is also due to my friends and colleagues in the department, as well as G&G staff and faculty for making my experience at Texas A&M University an enriching experience, both in education and personally.

A final thanks to my family for their patience, encouragement, and support through my studies.

TABLE OF CONTENTS

Page

LIST OF FIGURES

Page

CHAPTER I

INTRODUCTION

In the last few decades, the use and advancement of seismic attributes have been instrumental in improving the quality of reservoir characterization for hydrocarbon exploration and development. Petrophysical and lithological prediction are reservoir characterization tasks which can be aided by the analysis of seismic attributes such as reflector terminations, acoustic impedance inversion, and AVO (Chopra et al., 2003). The analysis of volumetric attributes, such as coherency and curvature, contributes towards describing the structure and shape of geological features of interest, such as faults, channels, and fractures from seismic data (Clumentritt, et al., 2003). It is these latter types of attributes that are of interest for fault/fracture characterization and the topic of this study: the applications of volumetric curvature and coherency attributes for the purpose of mapping fractures of the carbonate reservoirs in the Huabei oil field, North China.

The Huabei field is located on the Jizhong plain, in the central Hebei province, China, and extends to areas of Shandong, Tianjin, and Henan. Oil and gas exploration in Huabei oilfield began in 1955. The Renqiu oilfield - the largest Mesozoic burial-hill type carbonate oilfield in China – was discovered in 1975 (Zha, 1984). This study uses a 3D seismic data volume from one of the areas containing a carbonate reservoir in Huabei Oil Field. Fault detection within the carbonate reservoirs, using seismic attributes, can help to reduce the exploration risks and optimize production and drilling plans. Figure 1.1 shows the areal extent of the Huabei Field.

Figure 1.1 – Huabei Field, Northeast China. Carbonate reservoir in the field is target of our study.

Carbonate Reservoirs

Carbonate reservoirs are of great interest and importance to petroleum exploration, holding the majority of the world's oil reserves (60%) and nearly half of the world's gas reserves (40%). However, the recovery factor of hydrocarbon in carbonate reservoirs is lower than that in clastic rocks due to the increased complexity in pore types, structures, and their effects on porosity and permeability in carbonates. Therefore a heightened understanding of the faulting and resulting fractures which influence the different types of porosity and reservoir quality is advantageous to accurate reservoir characterization and prospect prediction.

Carbonate rocks are typically deposited in shallow, warm marine environments and are thus mostly biogenic in origin. They are comprised of two groups – limestones which are composed mostly of calcite ($CaCO_3$) and dolostones which contain mostly dolomite ($CaMg(CO_3)_2$. $CaCO_3$, or calcium carbonate, algae, coral, and other skeletal remains make up the grains of carbonate rocks. Due to the close proximity of carbonate deposition to the areas where carbonate grains are created, carbonate formations tend to be largely heterogenous. This heterogeneity is due to varying cementation rates and pore types in carbonates, as well as diagenesis occurring and results in high variability of lithological and petrophysical properties in carbonates. Our study will focus on the effects of physical and chemical diagenetic factors resulting in faults and fractures in carbonates towards predicting petrophysical properties.

Fractures in Carbonate Rocks

Intense fracturing is present and affects reservoir characteristics of some of the world's largest oil fields (Roehl and Choquette, 1985). The relationship between fractures and porosity/permeability is not clear due to the complexities of pore types in carbonates and the tendency of isolated porosity/permeability in small areas of a field. An example of such complex porosity is seen in Figure 1.2, where intergranular porosity is observed in thin section of the Andrews South Devonian field in West Texas.

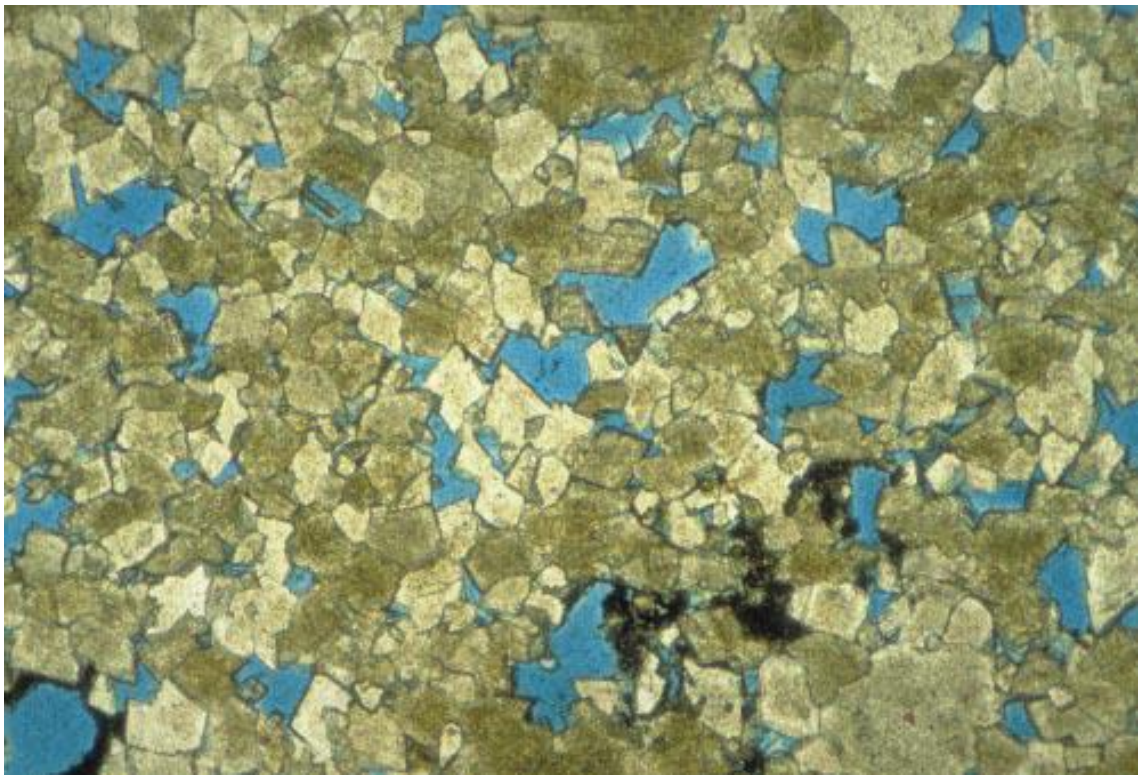

Figure 1.2 – Carbonate intergranular porosity observed in a thin section of dolowackestone, Andrews South Devonian field, West Texas. (Lucia, 1995)

Though there is not as clear a relationship between fracturing and porosity in carbonates as there exists in clastics, fractures do bring benefits to reservoir production. Fracture networks provide migration conduits for hydrocarbon, and karst, vuggy porosity which results from physical and chemical diagensis have been shown to be highly prone to hydrocarbon accumulation in carbonate rock.

Seismic Attribute Analysis

A seismic attribute is a measure or computational product of seismic data which is obtained in order to quantify geological features of interest (Brown, 1985). Interpreters may apply seismic attributes towards directly estimating geologic features and reservoir

properties, or defining the structural/depositional environment. Attribute analysis was first introduced in the early 1970s (Chopra and Marfurt, 2005) and is now widely used in reservoir prediction and analysis. Figure 1.3 shows several implementations of attribute analysis to identify meandering channels in seismic data.

Geometric attributes such as coherency provide interpreters a means to visualize and describe complex fault systems, fractures, salt and shale diapirs, and, in some cases, incoherent overpressured shales (Chopra, 2002). Volumetric curvature attributes can describe the presence of folds, anticlines, and fault zones, while assisting in the identification of fault features which fall below seismic resolution and detecting the fracture zones resulting from those faults. Used in conjunction, coherency and curvature provide the seismic interpreter additional tools for understanding the deformation and diagenesis processes in reservoirs. In carbonates especially, where diagenesis results in complex pore structures which strongly influence key reservoir properties of porosity and permeability, curvature and coherency analysis allows interpreters to map the fault systems to fracture density for reservoir prediction (Chopra and Marfurt, 2007a).

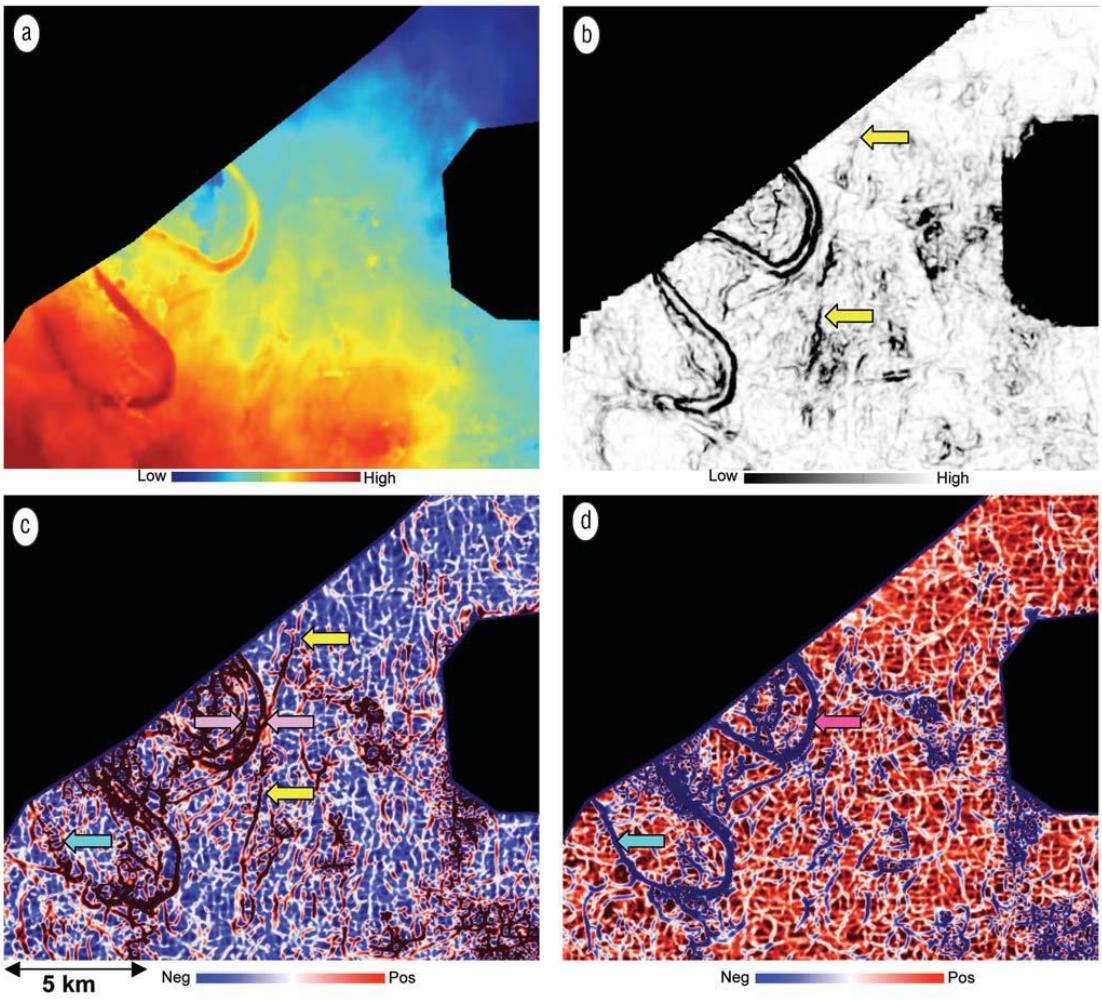

Figure 1.3 – Four implementations of seismic attribute analysis to describe river channels. (a) time surface; (b) coherence; (c) most-positive curvature; (d) most-negative curvature. Yellow arrows indicate the areas where curvature methods display better focusing of some features. Pink and blue arrows in most positive curvature show defined channel edges whereas the red and blue arrows in most-negative curvature indicate well-defined base of channel (Chopra and Marfurt 2007a).

Coherency

Coherency attributes quantify the similarity between seismic waveforms and traces (Chopra 2002). Due to the principle of convolution, these waveforms are the response of the acquisition wavelet convolved with the geologic response (Chopra and Marfurt, 2005). The resultant waveforms vary in amplitude, frequency, and phase, depending on the properties of the layers above and below the reflection interface. Such properties include facies type, density, porosity, and fluid type which contribute to the acoustic impedance of a depositional layer (Chopra and Marfurt 2007a). Thus, attributes extracted from processed seismic data and the analysis of these attributes provide interpreters valuable information for subsurface characterization. Coherent waveforms are indicative of uninterrupted lithology, while areas of low coherency can be the result of channels or faults (Chopra and Marfurt, 2007b).

One of the first coherency methods for identifying fault surfaces in a seismic volume was published by Bahorich and Farmer (1995). They calculated a coherence cube from seismic data by comparing seismic amplitudes on adjacent traces, a coherence calculation technique known as cross-correlation. On time and horizontal slices from the coherence cube, faults and other unconformities in seismic data could be clearly identified. Since then, other coherency analysis techniques such as semblance (Marfurt et al., 1998) and eigenstructure-based coherence (Chopra and Marfurt, 2007b) have been introduced and are widely used in industry and academia today.

Crosscorrelation

The crosscorrelation method operates by first identifying a master trace and a time window, then sliding a second trace by a number of time lags within that time window and cross-correlating the two traces (Figure 1.4). The time lag with the maximum signed

crosscorrelation value is designated the inline or crossline dip (whichever direction the second trace is in respect to the master trace). The crosscorrelation value, ρ_x which results from this peak time lag in the inline direction is then used with the maximum signed crosscorrelation value in the crossline direction, ρ_y, in equation (1.4) to calculate the 3D coherence estimate.

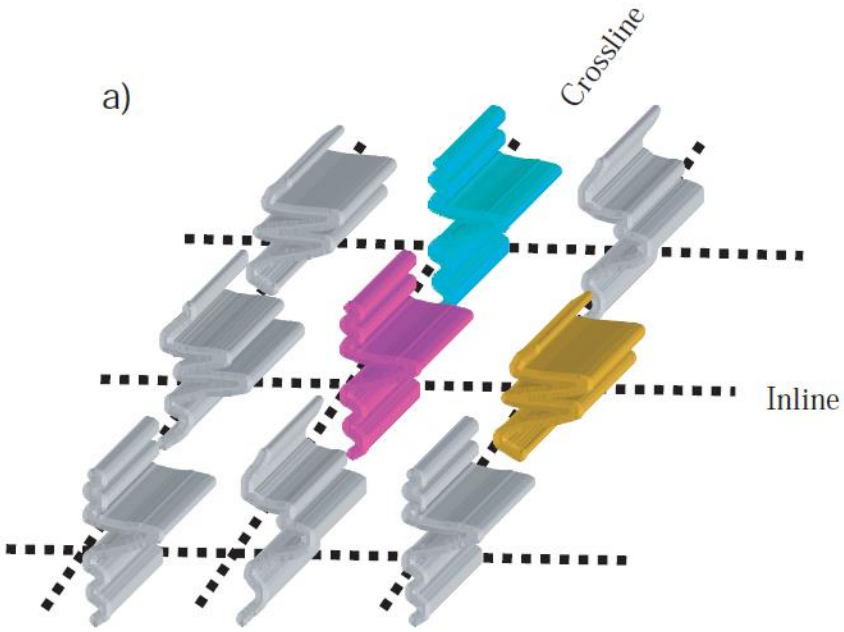

Figure 1.4 – Crosscorrelation method - Master trace (purple) is crosscorrelated to the adjacent inline trace (yellow) over a suite of time lags and obtain the maximum signed cross correlation value. This is repeated for the trace in the crossline direction (blue). The two peak crosscorrelation values are then applied to equation 1.4 below to calculate the 3D coherence estimate (Chopra and Marfurt 2007c).

the inline crosscorrelation coefficient is defined as:

$$\rho_x(t,\ \tau_x = \frac{\sum_{k=-K}^{+K}\{[u_0(t+k\Delta t)-u_0(t)][u_1(t+k\Delta t-\tau_x)-u_1(t-\tau_x)]\}}{\sqrt{\sum_{k=-K}^{+K}\{[u_0(t+k\Delta t)-u_0(t)]^2[u_1(t+k\Delta t-\tau_x)-u_1(t-\tau_x)]^2\}}} \quad (1.1)$$

where the n[th] trace running-window mean is defined as

$$< u_n > (t) = \frac{1}{2K+1} \sum_{k=-K}^{+K} u_n(t + k\Delta t) \tag{1.2}$$

the crossline crosscorrelation coefficient is defined as:

$$\rho_y(t,\ \tau_y) = \frac{\sum_{k=-K}^{+K}\{[u_0(t+k\Delta t)-u_0(t)][u_2(t+k\Delta t-\tau_y)-u_2(t-\tau_y)]\}}{\sqrt{\sum_{k=-K}^{+K}\left\{[u_0(t+k\Delta t)-u_0(t)]^2[u_2(t+k\Delta t-\tau_y)-u_2(t-\tau_y)]^2\right\}}} \tag{1.3}$$

By evaluating the corsscorrelation coefficients along the inline and crossline traces and determining the maximum signed coefficient values for each time suite of time lags, the 3D crosscorrelation coherence was estimated as follows:

$$c_{xc} = \sqrt{[\max_{\tau_x} \rho_x(t, \tau_x, x_i, y_i)[\max_{\tau_y} \rho_y(t, \tau_y, x_i, y_i)]} \tag{1.4}$$

where $\max_{\tau_x} \rho_x(t, \tau_x, x_i, y_i)$ means the cross correlation values at time lags τ_x when ρ_x is maxima while$\max_{\tau_x} \rho_x(t, \tau_x, x_i, y_i)$ means the cross correlation values at time lags τ_y when ρ_y is maxima.

The crosscorrelation estimate of coherence, by evaluating and using the maximum values of coefficients in both inline and crossline directions for their respective lags, this defnition for coherence accounts for local dip and is dependent only on waveform, not amplitude. As such, however, the crosscorrelation estimate is more sensitive to noise than the other estimates of coherence.

Variance

For the semblance and variance approach to coherence determination, an elliptical or rectangular space aperture is defined to evaluate the data in a time window. A futher condition of the semblance/variance calculation is that, unlike the cross-correlation estimate, a dip and azimuth must be determined for each point of analysis.

With the analysis window defined (rectangular or elliptical), containing J traces about a central analysis point, the semblance is defined as the ratio of the energy of the average trace to the average energy of all the traces along a given dip.

$$\sigma(t,p,q) = \frac{[\frac{1}{J}\sum_{j=1}^{J} u_j(t-px_j-qy_j)]^2}{\frac{1}{J}\sum_{j=1}^{J}\{[u_j(t-px_j-qy_j)]^2\}} \tag{1.5}$$

where j is the jth trace in the analysis window, x_j and y_j are the distances in the respective directions of the jth trace from the central analysis point. p and q are the apparent dips at time t in a planar event. The semblance σ denotes the similarity of the traces along this dip-defined plane inside the x,y aperture.

$$var(t,p,q) = \frac{1}{J}\sum_{j=1}^{J}\left[u_j(t-px_j-qy_j) - \langle u(t,p,q)\rangle\right]^2 \tag{1.6}$$

where the mean, $\langle u(t,p,q)\rangle$ is

$$\langle u(t,p,q)\rangle \equiv \frac{1}{J}\sum_{j=1}^{J} u_j(t-px_j-qy_j) \tag{1.7}$$

$\langle u\rangle$ is calculated for each plan parallel to the reflector with the analysis window. Equations (1.6) and (1.7) provide the formal definition of variance, however, most statisticians use the much more efficient computational form

$$var(t,p,q) = \frac{1}{J}\sum_{j=1}^{J}\left[u_j(t-px_j-qy_j,x_j,y_j)\right]^2 - \left[\frac{1}{J}\sum_{j=1}^{J}\left[u_j(t-px_j-qy_j,x_j,y_j)\right]\right]^2 \tag{1.8}$$

which is also mathematically equivalent to the formal one. To estimate coherence, we sum the variance over a vertical analysis window of 2K+1 samples and normalize by the energy of all the traces to obtain

$$c_v(t,p,q) \equiv \frac{\sum_{k=-K}^{+K}\frac{1}{J}\sum_{j=1}^{J}[u_j(t+k\Delta t-px_j-qy_j)]^2 - \sum_{k=-K}^{+K}\left[\frac{1}{J}\sum_{j=1}^{J}[u_j(t+k\Delta t-px_j-qy_j)]\right]^2}{\sum_{k=-K}^{+K}\frac{1}{J}\sum_{j=1}^{J}[u_j(t+k\Delta t-px_j-qy_j)]^2} \tag{1.9}$$

or

$$c_v(t,p,q) \equiv 1 - \frac{\sum_{k=-K}^{+K}\left[\frac{1}{J}\sum_{j=1}^{J}[u_j(t+k\Delta t-px_j-qy_j)]\right]^2}{\sum_{k=-K}^{+K}\frac{1}{J}\sum_{j=1}^{J}[u_j(t+k\Delta t-px_j-qy_j)]^2} = 1 - c_s(t,p,q) \quad (1.10)$$

We are given a larger number of traces to correlate to a mean trace and thus gain angular resolution over the crosscorrelation estimate, variance is sensitive to changes in both waveform and amplitude.

Eigenstructure-based Coherence

Eigenstructure-driven coherence estimation addresses the drawbacks of both semblance/variance and cross correlation coherence estimations. Semblance is sensitive to both waveform and lateral changes in seismic amplitude. When delineating complex faults and fractures through a seismic volume containing other geologic features which have similar seismic reflection responses as those faults, it becomes difficult for variance estimation to differentiate between the two features. Additionally, while the cross-correlation estimation of coherence is only sensitive to waveform and not amplitude, it is increasingly sensitive to noise. When using seismic attributes, it is advantageous to use attributes which are mathematically independent of each other (Barnes and Laughlin, 2002), or in other words, only measure one property of the seismic response. These separate analyses can then be combined later to assist in the identification of target features. By eigenstructure analysis, waveform and amplitude of a seismic response can be separated into two mathematically independent covariance matrices which then can be analyzed separately.

The eigenstructure method analyzes a window of traces and determines the wavelet which best demonstrates the changing waveform. Once this wavelet is determined, it is then scaled to fit each trace, which results in the representation of the coherent component of the

data. The eigenstructure coherence is equivalent to the ratio of the energy of this coherence component to the energy of the initial traces.

Taking each column of the data matrix and cross-correlating those columns with one each other column, we define a covariance matrix:

$$c_{ij}(t,p,q) = \sum_{k=-K}^{+K}\left[u_i\left(t + k\Delta t - px_j - qy_j\right) - \mu(t,p,q)\right]\left[u_j\left(t + k\Delta t - px_j - qy_j\right) - \mu(t,p,q)\right] + \sum_{k=-K}^{+K}\left[{u_i}^H\left(t + k\Delta t - px_j - qy_j\right) - \mu^H(t,p,q)\right]\left[{u_j}^H\left(t + k\Delta t - px_j - qy_j\right) - \mu^H(t,p,q)\right] \quad (1.11)$$

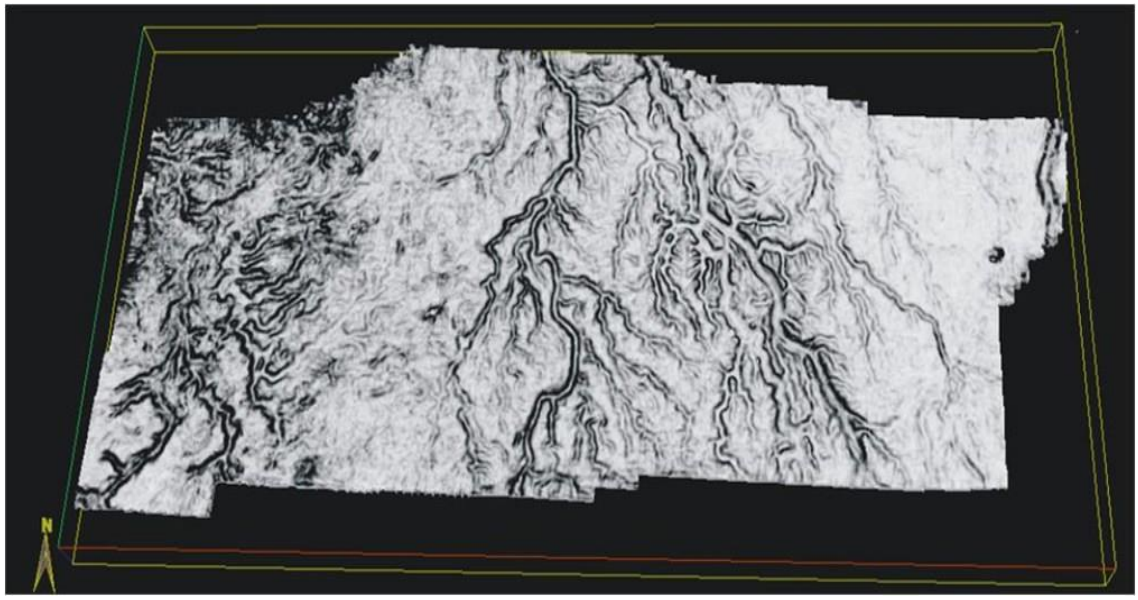

Figure 1.5 – Eigenstructure coherence calculation with PC (Primary Component) filtering along horizon slice. Channel edges are clearly visible (Arcis).

Sensitivity of Coherence to Dip and Window Size

One benefit of using seismic coherence for attribute analysis is that there exists only a few parameters to adjust in each implementation of calculating the coherence. Those include a dip calculation/search, vertical analysis window size, and the spatial aperture. Understanding the effects of each of these parameters is of great importance when performing attribute analysis as calculation time, efficiency, and accuracy are dependent on selecting the correct parameters.

The dip correction or scan is a critical step in coherence determination for most datasets. Commercial software such as Petrel and Landmark calculate coherence with an option to automatically scan for the structural dip estimate. Other software suites allow the interpreter to manually enter the maximum reflector dip through the dataset. If this is inaccurately entered, the coherence algorithm may search for a dip that is unrealistically large for the dataset, which leads to steeply dipping background noise being misidentified as coherence reflectors.

The spatial aperture affects the calculation time and angular resolution of the coherence result. A larger spatial analysis window will result in increased angular resolution and at a certain depth, begin to decrease the lateral resolution. Due to attenuation of seismic waves with depth, the frequency spectra values decrease with depth, and thus it is best to use a smaller spatial aperture for shallow targets, while deeper targets should be analyzed with a larger window.

Evidence for this is shown in Figure 1.6, where it is observed that with a smaller spatial window size (12.5m = 5 traces), increased lateral resolution of channels are observed

in (a), yet muted in (b), (c), and (d). It should be noted the increased angular resolution with a larger spatial radius (>12.5m) in the meandering channel detail.

Time analysis-window size also has a significant effect on coherence calculations. Larger window sizes are more likely to stack more uncorrelated geologic data into one analysis window, which depreciates coherence image and blurs the stratigraphic details. Prior work has shown that for thin channels, the optimal time window size is the reciprocal of the dominant frequency (Blumentritt et al. 2003).

The tradeoff is that shorter time windows were more contaminated by noise; thus for some applications, using a longer window which may yield blurred stratigraphic features, may be the best implementation as these mixed geologic features are at least without noise. Furthermore, larger vertical analysis windows are better at identifying vertical faults, as the coherence calculation stacks similar discontinuities through a longer temporal window. These points are illustrated in Figure 1.7.

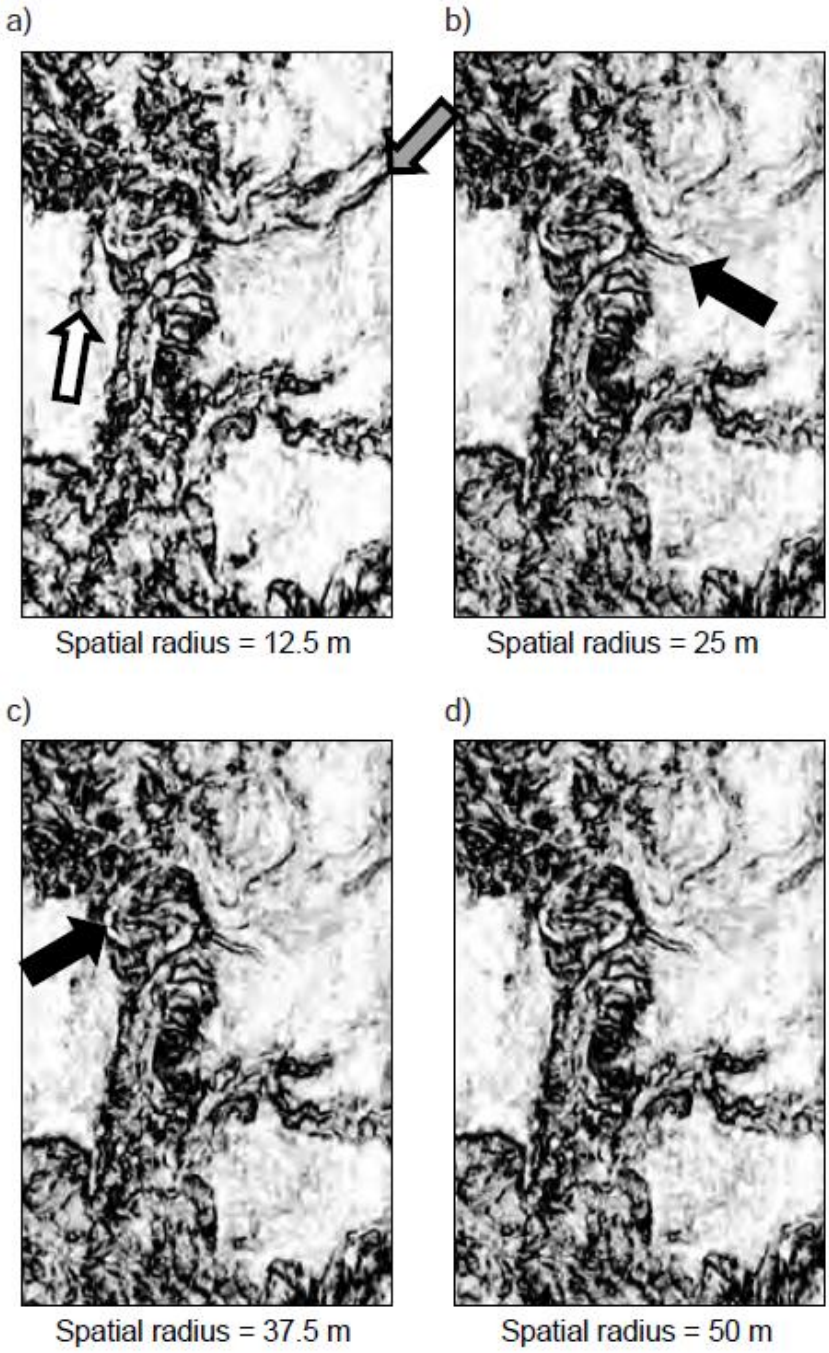

Figure 1.6 – The effects of increasing spatial aperture on coherence calculations, fixed time window of 16ms. Note that while (a) shows the thin feature described by the white arrow, it also most accurately depicts the wide channel (grey arrow). In contrast, the intermediate channel denoted by the black arrow shows in (b), (c) and (d), when the spatial aperture is larger than 12.5m (Chopra and Marfurt 2007d).

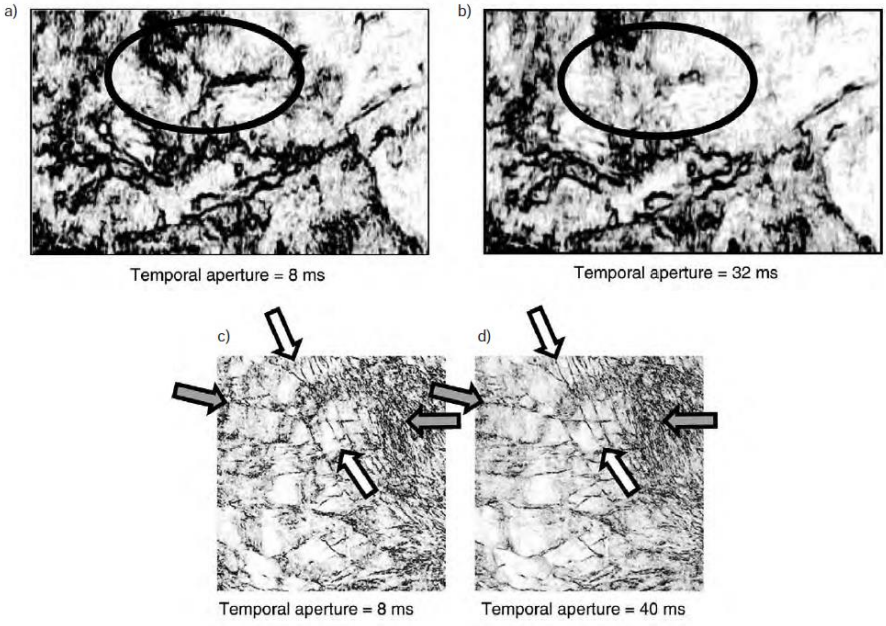

Figure 1.7 – Effects of changing temporal analysis window. Larger time windows for analysis will tend to blur stratigraphic features (black circles) due to certain stratigraphic features which may be confined to a geologic horizon. The larger time windows, however, improve the appearance of vertical faults in (c) and (d), due to the coherence calculation stacking similar discontinuities over larger windows (Chopra and Marfurt 2007d).

Curvature

Curvature in Potential Field Theory

Many exploration methods with geophysical foundations are based in potential field theory and gridding; cuvature happens to be one such example. This gridding allows interpreters to represent the original scattered data points on a regular grid. Minimum curvature interpolation operates under the elastic-plate flexure model, in attempt to fit seismic data to a 2D cubic spline (Love, 1927). Small displacements f of the elastic plate are described by:

$$\eta \frac{\partial^2}{\partial x_j^2} \frac{\partial^2 f(x_i)}{\partial x_i^2} - \left(T_{xx} \frac{\partial^2 f}{\partial x_1^2} + T_{xy} \frac{\partial^2 f}{\partial x_1 \partial x_2} + T_{yy} \frac{\partial^2 f}{\partial x_2^2} \right) = q \tag{1.12}$$

Equation (1.12) has special cases such as minimum curvature gridding equation. For instanse when the horizontal forces are zero we obtain:

$$T_{xx} = T_{xy} = T_{yy} = 0, \tag{1.13}$$

and g=η/q, we obtain

$$\frac{\partial^2}{\partial x_j^2} \frac{\partial^2 f_k}{\partial x_i^2} = g_k \delta(x - x_{i,k}), \tag{1.14}$$

Where the g_k is the strengths of point loads on the elastic plate, δ is the Kronecker function and $x_{i,k}$, $f_k = f(x_{i,k})$ are the constraining data. The g_k must be chosen in the same way of $f \to f_k$ as $x_i \to x_{i,k}$. The g_k Mathematically are the coefficients of a linear combination of Green's function.

Furthermore, this solution was required to fulfill three free-edge boundary conditions and they are as follows: First, on the edges, the bending moment must be zero,

$$\frac{\partial^2 f}{\partial n_i^2} = 0 \tag{1.15}$$

Second, the vertical shear stress must also vanish on the edges,

$$\frac{\partial}{\partial n_i} \frac{\partial^2 f}{\partial x_j^2} = 0 \tag{1.16}$$

and last at the corners the twisting moment must be zero,

$$\frac{\partial^2 f}{\partial x_i^2} \tag{1.17}$$

where n is a unit vector normal to the edge. The unique solution of equation (1.14) with these conditions and continuous second dericatives is the natureal bicubic spline.

Briggs (1974) found that the norm

$$C = \iint \left(\frac{\partial^2 f(x_i)}{\partial x_i^2}\right)^2 dx_1\, dx_2, \tag{1.18}$$

can be minimized if a function f obeys equation (1.14), and vice versa. Because the equation (1.18) is a valid approximation for the total curvature of f when $\frac{\partial f}{\partial x_i}$ is small, it is designated the minimum curvature.

Two and Three Dimensional Curvature

Two dimensional curvature is defined as the radius of the circle tangent to a curve (Sigismondi and Soldo, 2003), which is extracted to a target horizon of interest for attribute analysis. Fractures result from the bending of brittle rocks, which result in lithological discontinuities in reflection seismic data. The amount of bending can be quantified as curvature and thus, curvature attributes can be used to assist other attribute analysis techniques, such as coherency, in fracture detection (Chopra and Marfurt, 2007c). The curvature definition, applied to three dimensions, allows for a volumetric curvature cube to be generated, which provides valuable information on fracture orientation and density in zones where seismic horizons cannot be easily picked (Chopra and Marfurt, 2003).

Lisle (1994) was among the first to discover the correlation between seismic curvature values and measured fractures from outcrop. Following this discovery, different curvature methods (Gaussian, strike, dip, etc) have all been shown by different workers to be highly correlated with fractures in outcrop (Hart, 2002; Ericsson et al., 1988; Sigismondi and Soldo, 2003; Massaferro et al., 2003); Al-Dossary and Marfurt (2006) established the volumetric curvature technique for extracting curvature in three-dimensional seismic. Prior curvature analysis for fracture identification was taken along stratal slices of seismic data (Roberts, 2001) which require interpretation time and accuracy in horizon determination.

Curvature Types

Using least-squares fitting to approximate a quadratic surface,

$$z(x,y) = ax^2 + cxy + by^2 + dx + ey + f \tag{1.19}$$

We rotate the coordinate systems (Roberts 2001) to define:

Mean curvature:

$$k_{mean} = [a(1+e^2) + b(1+d^2) - cde]/(1+d^2+e^2)^{3/2} \tag{1.20}$$

Gaussian curvature:

$$k_{Gauss} = (4ab - c^2)/(1+d^2+e^2)^2 \tag{1.21}$$

The principal curvatures:

$$k_1 = k_{mean} + \left({k_{mean}}^2 - k_{Gauss}\right)^{1/2} \tag{1.22}$$

$$k_2 = k_{mean} - \left({k_{mean}}^2 - k_{Gauss}\right)^{1/2} \tag{1.23}$$

k_{mas} and k_{min} represent the maximum and minimum curvatures which are related inversely proportionally to the radius of two orthogonal circles curvature mentioned above. k_{mas} and k_{min} are defined as:

$$k_{max} = \begin{cases} k_1 \; if \; |k_1| \geq |k_2| \\ k_2 \; \; if \; |k_1| < |k_2| \end{cases} \tag{1.24}$$

and

$$k_{min} = \begin{cases} k_2 \; if \; |k_1| \geq |k_2| \\ k_1 \; \; if \; |k_1| < |k_2| \end{cases} \tag{1.25}$$

The most-positive curvature is defined as

$$k_{pos} = (a + b) + [(a - b)^2 + c^2]^{1/2} \tag{1.26}$$

and the most-negative curvature is defined as

$$k_{neg} = (a + b) - [(a - b)^2 + c^2]^{1/2} \tag{1.27}$$

Volumetric Curvatur

The first and second derivatives of equation (1.19) at x=y=0 in order to calculate the coefficients of a, b, c, d, and e can be evaluated by using the input estimates of reflector dip, $p = \frac{\partial z}{\partial x}$ and $q = \frac{\partial z}{\partial y}$:

$$a = \frac{1}{2}\frac{\partial p}{\partial x} \tag{1.28}$$

$$b = \frac{1}{2}\frac{\partial q}{\partial y} \tag{1.29}$$

$$c = \frac{1}{2}\left(\frac{\partial p}{\partial x} + \frac{\partial q}{\partial y}\right) \tag{1.30}$$

$$d = p \tag{1.31}$$

$$e = q \tag{1.32}$$

A crude measure of mean curvature were calculated by Marfurt and Kirlin (2000) as:

$$k_{mean} = \frac{1}{2}\left(\frac{\partial p}{\partial x} + \frac{\partial q}{\partial y}\right) \tag{1.33}$$

the rotation was defined as:

$$r_z = \frac{\partial p}{\partial y} - \frac{\partial q}{\partial x} \tag{1.34}$$

Previous Attribute Analysis in Huabei Field and Similar Carbonate Fields

Correlating production to curvature in carbonates was first explored by Ericson, et al (1988) in their work on a Cretaceous carbonate reservoir in New Mexico. Studies going forward involved exploring the types of curvature and dip calculations (Marfurt and Kirlin, 2000) anhd their best applications in carbonates of differing fracture types and porosities (Nissen, et al., 2009).

Prior work in the Huabei field focuses on characterization of the carbonate reservoir and predicting the fault network for prospect evaluation. As porosity in carbonates is closely related to the diagensis and faulting through the field, the resulting fracture network, presence of karst/vuggy porosity, and interconnectivirty of the fractures are strong indicators of hydrocarbon reservoirs. The average of maximum curvature and negative curvature is found to be directly correlated to fracture density from well data throughout the Huabei field (Han, et al., 2011). Coherency calculations are used in this work to confirm the curvature results when compared to the seismic data.

Production from the Huabei oil field has contributed greatly to the commerical oil productivity in China since its discovery in 1955, peaking in 1978. Since then, the field has maintained 10 million tons of oil production per year until 1986, with over 47 oil fields developed through the region. Since this time, the Huabei field production has decreased, but due to the size and quality of the unproduced regions, it still remains an important oil field for China's current and future commerical oil production interests.

Statement of Problem

Though it is established that fractures are beneficial for hydrocarbon identification and production from carbonate reservoirs, the resulting porosity and permeability are difficult to predict due to complexities in pore structures and types in carbonates. Heavy fracturing can also be difficult to identify on seismic alone if the fractures fall below seismic resolution. Alternate techniques must be explored and applied toward assisting fracture identification in carbonates.

Seismic attribute analysis-aided interpretation is still one of the key methods for lithological and petrophysical description of potential reservoirs. As we transition from easy, abundant discoveries in conventional reservoirs to unexplored frontiers with complex geology, such as densely-fractured carbonate reservoirs, we must rely on evolving existing techniques for improving the accuracy of geological interpretation in these complex fields. Advancements in data acquisition and processing methods must be matched by similar advancements in attribute analysis techniques to improve the accuracy of reservoir characterization. Such advancements must be met with comprehensive understanding of each method for efficient and effective application in seismic interpretation, reservoir characterization, and fault identification.

Volumetric curvature and coherency have been at the forefront of attribute analysis advancements for fault/fracture identification and mapping in seismic interpretation for the past several decades. These and other relevant attributes should be used together to improve the understanding of fractured carbonate reservoirs and identify exploration prospects. Methods of calculating these attributes must be understood, adjusted, and applied in a case-by-case approach to different datasets. Obtaining accurate, quantifiable attributes in a

specific field study is valuable towards the production or research goals in the field. More valuable, however, may be discovering an empirical relationship between the attribute and carbonate reservoir well data which can be applied or referenced to in production strategies in analogous reservoirs; thus the motivation behind our investigation in the Huabei field.

My thesis research will investigate the options in coherence and curvature attribute analysis available to us for fault and fracture description in a carbonate reservoir of the Huabei field. Specifically, the parameters of coherence and curvature determination from seismic data will be tested, applied, compared, and evaluated to zones of low impedance to determine their effectiveness in describing specific zones of interest in a prospective carbonate reservoir of Huabei field.

Research Objectives

To address the scientific problems stated for this research, we will investigate the volumetric attribute analysis techniques of coherence and curvature for carbonate reservoir fault description. This study integrates geology and geophysics via interpretation-driven formulation of attribute-extraction techniques for reservoir characterization as follows:

1. Identify the lithology and general trend of faulting in the field from interpretations of low and high-resolution seismic volumes.
2. Analyze the methods of coherency calculation and various parameters involved in volumetric curvature extraction for application towards areas of minor faulting and predicted fracture density in the field, and determine the best methods to apply through the dataset to most accurately describe these fracture networks.
3. Obtain the volumetric curvature and coherency maps which, together with high-resolution seismic, and P-wave impedance inversion results, aid in the interpretation of

the fracture network through the field.

Determining, adjusting, and applying the coherency and curvature algorithms which best depict the minor fault networks in the dataset is integral to both obtaining an improved interpretation for reservoir characterization in the field and producing an accurate correlation to petrophysical attributes indicative of fractures (P-wave impedance) derived from exploration well data.

This preliminary work in the Huabei field used exploration well data in attempt to describe the areas of minor faulting and predicted fracture density for reservoir characterization and possible prospect identification in a complex carbonate reservoir. Our study area of the Huabei Field encompasses such an area which has not yet been produced from, with several exploration wells drilled in the southern region. Through knowledge of the geologic and tectonic history of the field, exploratory wells have been drilled mainly in the southeastern section of the field, where complex faulting is known to exist and resulting dense fractures/improved reservoir conditions are assumed. As some of these exploratory wells contained intervals of hydrocarbon shows, the motivation for further exploration and possible production is heightened. This same motivation drives the goals of our research: to examine the relationship between seismic attributes and the fault networks/fracture density in the region's carbonate reservoir and, together with well-dervied impedance inversion, establish these attributes as direct hydrocarbon indicators in complex carbonate reservoirs.

It is our hope that our findings in applying volumetric curvature and coherence attribute analysis to this region of the Huabei dataset can be used to both reduce the risk in prospect identification for the heavily faulted southeast region of the area and provide the blueprint for establishing an empircal relationship between seismic attributes and

hydrocarbon-conducive fracture density for possible exploration targets in the northern area of the field. Meeting these goals could encourage production efforts and further exploration in this region of the Huabei field, which extends the productivity of the field. Furthermore, any relationships we discover between seismic attributes and hydrocarbon-yielding fractures can be applied in analagous carbonate fields through the world.

CHAPTER II

METHODOLOGY

Data Interpretation and Conditioning

A low (15 Hz) and high (60 Hz) resolution seismic dataset is obtained from the Huabei oil field. Sandstone overlays the carbonate reservoir in the field; varying degrees of major and minor fault density are observed in both the low and high resolution volume. The top of the carbonate reservoir in the field is interpreted, and with well log data, impedance inversion is used to verify most of the high-resolution seismic results to be structurally significant. The resulting volumes are conditioned with dip-guided structural smoothing and edge enhancement to accentuate the continuities and discontinuities (faults, fractures, folds) in seismic reflectors. This conditioning prepares the data for volumetric curvature and coherence attribute analysis and following fault/fracture delineation.

Horizon Interpretation

The Petrel software platform is used for interpretation of the top of the carbonate reservoir in the field area. The reservoir depth and top are determined from well log and production data. The horizon is interpreted to an 8 x 8 density and then interpolated as a surface to be used in the coherence and curvature calculations. We denote this surface Reservoir Top and will refer to it as such in the report. Production data from wells indicate the depth at which the carbonate reservoir begins, and this is used to interpret this Reservoir Top surface through the field.

Volume Calculation Time Considerations

The workflow for calculating seismic attributes and extracting the attribute values to a surface is to first calculate the volume attributes from the seismic cube to obtain an attribute cube and then extract the values of that cube onto a designated surface in Petrel/Seisworks.

Due to the size of the field (1540 lines x 829 traces or ~ 501km^2), disk size for both volumes, and amount of calculation time, it is impractical, especially when testing different seismic attribute analysis parameters, to obtain the desired attribute over the entire volume. Therefore, for comparison and analysis, we first identify the areas in the field and reservoir which are of structural, dimensional, or production interest and crop the volume to fit these smaller areas. The subsequent testing of attribute analyses methods, parameters, and generation of seismic attribute cubes for these cropped volumes can then be completed in a reasonable amount of time.

Comparison of Horizon Curvature and Coherence to Low Impedance-Inversion Zones

Once the optimal attribute analyses methods are determined for the interpretation of different geological targets (major faults, small-scale faults, possible fracture zones), we apply the respective attribute analysis methods to the Reservoir Top horizon in 5ms incremental time horizon slices deep to the Reservoir Top in the high resolution volume. On these horizon time slices, we extract the seismic attribute of interest for major/minor fault description and analyze them in zones of inversion-generated low P-wave impedance by Zhang et al. (2014). Low impedance zones could be indicators of high fracture density, as heavy fracturing decreases both density of the rocks and the velocity of the waves

transmitted through them. Other possible explanations of low impedance can be the presence of a rapid depositional change or unconformities. From Reservoir Top to +140ms horizon time (increasing depth), we identify and interpret zones of low impedance most likely due to minor faulting/fracturing, and analyze those interpretations by comparing the corresponding seismic attribute results in these zones.

Subvolumes and Analysis Motivation

We crop three sub-volumes from our dataset for determining which attributes best describe the features of interest and for testing the optimal parameters to be used in calculating those attribtues. The first, from the northeast section of the field, inline 1700 to 1900, crossline 2421 to 2721, 3500 ms to 5000 ms (where our reservoir top exists), an area of 24 km^2 where general East to Northeast trending faulting exists. This sub-volume is selected for analysis of the lower fault/fracture density away from the wells and production are. Our aim is to determine whether the coherence attribute calculation methods available in Petrel can identify medium-scale, uniform-direction faulting at the reservoir depth, away from production zones.

The second sub-volume is a cropped volume from the entire field, focusing on the shallower depths, 1040 to 2580 inline and 2421 to 3250 crossline, 500 ms to 1500 ms. This region includes the structure in the shallow regions of our field, above the reservoir. For this subvolume, we are interested in the large regional NEE trending fault which exists at shallow depth through the center of the field. Our aim is to obtain a depiction of large-scale faulting in terms of the coherence attribute in Petrel.

The third volume will be the subvolume containing our production interests, from 1640 to 2040 inline and 3020 to 3250 crossline, 2000ms to 4000ms, where heavy faulting

and fractures exist, as well as the majority of wells drilled in the Huabei field. This is the area where the most strenuous coherence parameter testing will be performed to try and describe the regional faults and the resulting fracture networks.

Volumetric Curvature and Coherency Methods in Petrel and Landmark

To delineate the faults and fractures in greater detail and accuracy than the seismic alone can show, volumetric curvature and coherency methods are applied through the dataset. We will use the most positive and most negative curvature values for the majority of the data volume and alter the curvature calculation in areas with high fracture density as needed. Similarly, through most of the dataset, a five-trace semblance coherency calculation will be used to describe the general faulting, with adjusted parameters, eight-trace eigenstructure, and ant-tracking algorithms applied in areas with high fracture density. Once the optimal parameters have been determined, the respective curvature and coherency methods will be applied to the high-resolution data.

Petrel Coherence Calculations and Parameter Testing

The earlier coherence calculation methods of cross-correlation and semblance, previously mentioned and described by Chopra and Marfurt (2007b), are included in most conventional interpretation software suites, including Petrel and Landmark. Petrel's volume attribute calculation requires a seismic volume as input. Our first step is to apply dip-guided structural smoothing with edge enhancement on the original data, which increases the continuity of the seismic reflectors parallel to local structure orientation estimates, while enhancing the detected edges in the seismic. This conditions the seismic data for coherence calculations to more clearly define the incoherent data areas and associate those to faults and

fractures.

Cross-Correlation in Landmark

Coherence measures are all calculated for a defined spatial window. The most basic coherence calculation correlates a single adjacent trace to a master trace from the inline and crossline directions: an evaluation of coherency from three traces, or the three-trace crosscorrelation method. This is done through Landmark Seisworks which allows the calculation of seismic attributes from user-defined volumes. Input options range from using the entire volume, to a user-defined time window. To minimize calculation time, we opt to use a volume defined by a time window +/- 40 ms above and below the top of the reservoir horizon.

Variance in Petrel

Recalling that variance is defined as

$$var(t,p,q) = \frac{1}{J}\sum_{j=1}^{J}\left[u_j\left(t - px_j - qy_j\right) - < u(t,p,q) >\right]^2 \tag{2.1}$$

where the mean $< u(t,p,q) >$ is defined as

$$< (u,t,q) \geq \frac{1}{J}\sum_{j=1}^{J} u_j(t - px_j - qy_j) \tag{2.2}$$

In Petrel, we test for different values of J by adjusting the number of inline by number of crossline traces we wish to evaluate the variance along (spatial aperture). Also, we are given the option to compensate for dip, which is completed in a separate, calculation-intensive dip scan through the volume. We are further given the option to test for a vertical smoothing parameter, which most closely translates to the temporal window (though not an

analysis window definition).

Eigenstructure-driven Coherence in Landmark

In Landmark, we are given the option to calculate eigenstructure-based coherence for a volume input. We choose the input to be the volume defined by +/- 20ms above and below our reservoir top horizon, which is imported from Petrel.

Volumetric Curvature in Landmark

Volumetric curvature in Landmark is calculated as a curvature attribute analysis. As we are able to select a horizon as the input parameter, this curvature calculation can be defined as volumetric in theory. From literature review, the most suitable curvature estimation for delineating faults and fractures is the most-positive and most-negative curvatures.

Correlating Attribute Data to Low-Impedance Zones

Upon obtaining volumetric curvature and coherency volumes from the high resolution seismic volume, these values are extracted along Reservoir Top and analyzed with P-wave impedance results from well log data inversion. Along with an understanding of the geology/deposition in the region at reservoir depth, we can use these two pieces of information to predict and validate the presence of fractures in specific areas through the reservoir. This relationship between seismic attribute, well-log inversion impedance, and presence of minor faults/fractures can be applied away from the well locations through the field and be used as a predictor of fracture density in the carbonate reservoir.

CHAPTER III

LOW RESOLUTION (15Hz) DATASET ATTRIBUTE ANALYSIS

Introduction

In this chapter, we apply the seismic attribute analysis techniques of coherence and curvature to the low-resolution (15 Hz) seismic volume to assist in fault/fracture determination. We determine the optimal parameters for each coherence (variance, cross-correlation, eigenstructure) calculation and generate the volumetric curvature attributes to assist in the interpretation. As curvature has been shown to better define the smaller faults and fractures in outcrop, the curvature maps can be used alongside the coherence results to describe regional faulting and isolated fracture networks.

As these calculations must be done with commercial software packages of Schlumberger's Petrel and Halliburton's Landmark, it is burdensome, but necessary, to take processor speed, disc space, and calculation time into account. These considerations, however, align with the necessity in exploration and production to find the most time and cost efficient means of completing an assessment or objective.

Data Interpretation and Conditioning

We begin by first conditioning the datasets by cropping them into sub-volumes to isolate areas of geologic and production interests as detailed previously. We test the coherence calculation parameters for each sub-volume, taking note of which parameters work better at varying depths and fracture densities. Then, with Landmark, we test the cross correlation and eigenstructure coherence methods, as well as volumetric curvature.

Coherence Parameter Testing

Petrel's coherence analysis options are limited to calculating variance alone. Thus, we will test the parameters for Petrel's variance algorithm for each subvolume, then test the parameters for cross-correlation and eigenstructure coherence in Landmark. In doing so, we are able to visualize the effects of altering the aperture window size and analysis time window on seismic data.

As previously mentioned, variance is essentially equivalent to one minus the semblance calculation of coherence. Both measures are evaluations of how well each trace fits the mean trace along the dip, if defined. In Petrel, we are given the option to manipulate the spatial aperture size (from 1x1 to 11x11), and the vertical smoothing parameter (from 0-200), as well as indicate whether to calculate the dip-correction.

We use the cropped volume from the production area, labeled subvolume C, to test the variance parameters which yield the best results for fault and fracture delineation. This subvolume is selected because it is in our production zone of interest, and at reservoir depth. Thus, if we obtain the parameters which best represent the variance, or lack of correlation, which describe regional faults and fracturing, we can apply these parameters to the variance estimation through the field.

We test the production sub-volume C for different values of spatial aperture ranges, vertical smoothing, and dip correction. The approach we used is to test the extremes for aperture size, then adjust the vertical smoothing to find the best depiction of the faulting in the region. We also toggle the dip-correction option to observe the effects of accounting for dip in the data volume calculation.

Results

Crosscorrelation

In Landmark, we generate a 3-trace cross correlation estimate of coherency along our target horizon using a temporal aperture of 200ms. We observe greater detail in the imaging of the general faulting in the area, as well as in our production area when compared to the variance calculation in Petrel. Though it is variance which should be less sensitive to noise, we actually observe a sharper image in the crosscorrelation estimate (Figure 3.1). This is perhaps due to the vertical smoothing factor, inaccurate dip search, or simply a lower resolution in Petrel's visualization capabilities.

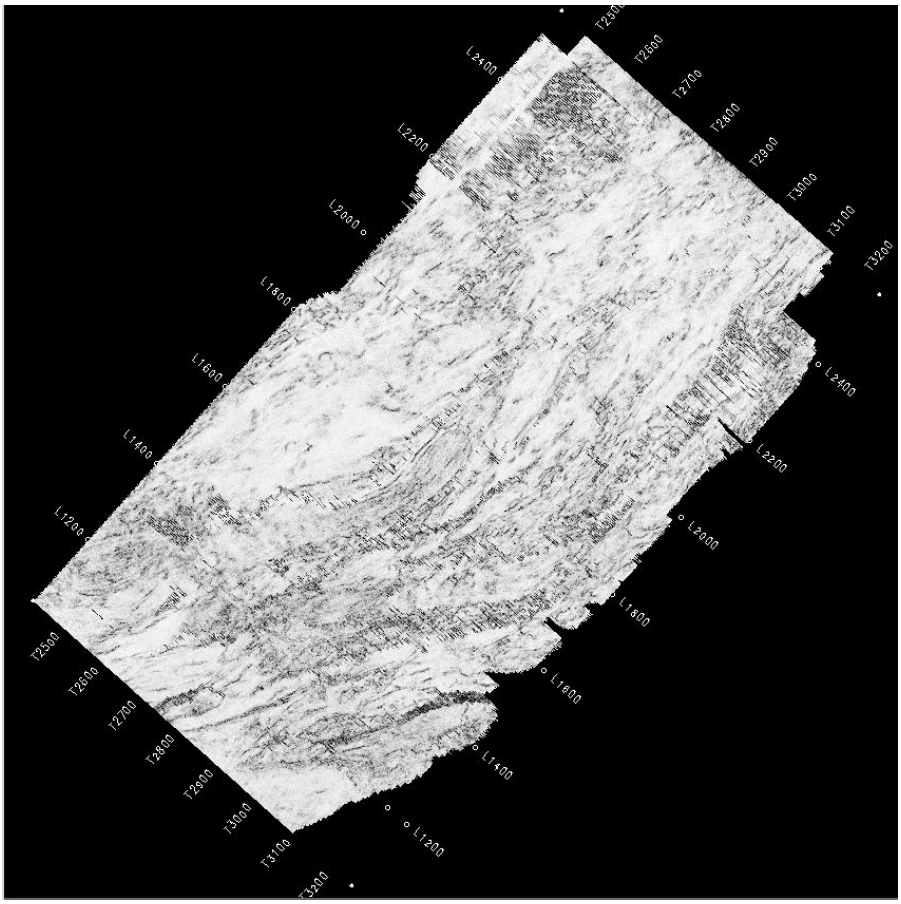

Figure 3.1 – Crosscorrelation Coherence Low Resolution, Reservoir Top Horizon – Spatial aperture 3x3, temporal window 200ms.

Variance

We find that for subvolume C, using a spatial aperture of 2x2 traces, vertical smoothing of 47, with dip correction, we obtain the best results for mapping the faults and fractures in the production area along the top of the horizon. Though the images suffer from resolution loss due to zooming in, the variance calculation nevertheless accurately reflects the areas of low coherence, where faulting and fracturing in the production area exist. We can observe this when the variance values are extracted to the reservoir top horizon and

compared to the seismic inline 1050, as seen in Figure 3.2. The complex faulting and other reflection discontinuities are shown in the variance volumes along the horizon top strata.

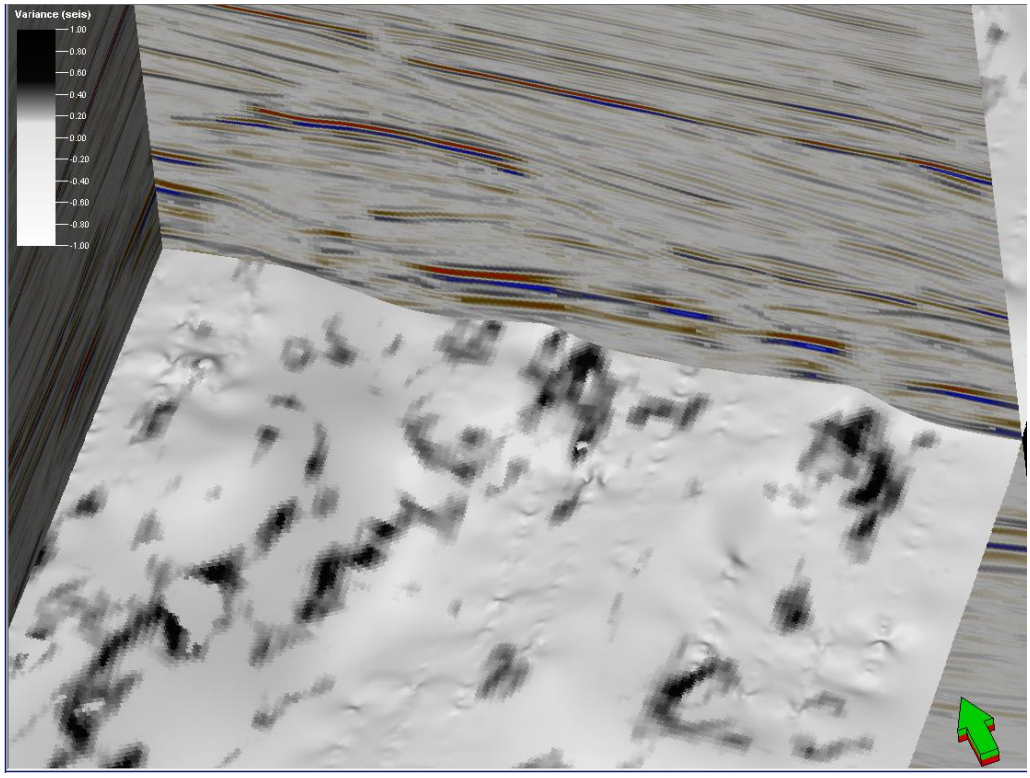

Figure 3.2 – Variance values extracted to Top Reservoir horizon. Despite the loss of resolution due to zooming in, the areas of seismic discontinuities above the horizon from seismic inline 1050 are reflected as high variance zones.

These variance parameters are applied to structurally smoothed, edge-enhanced subvolume A, as shown in Figure 3.3. In subvolume A, we observe that variance parameters of a 2-trace inline x 2-trace crossline aperture with vertical smoothing of 47 and dip correction shows the general faulting trend through a timeslice at 4000ms (near the reservoir depth in this area). The variance volume does also suffer from resolution loss due to zooming in, but most areas with complex faults and fracture density are still captured,

similar to the results from subvolume C and shown in the circled areas of Figure 3.3.

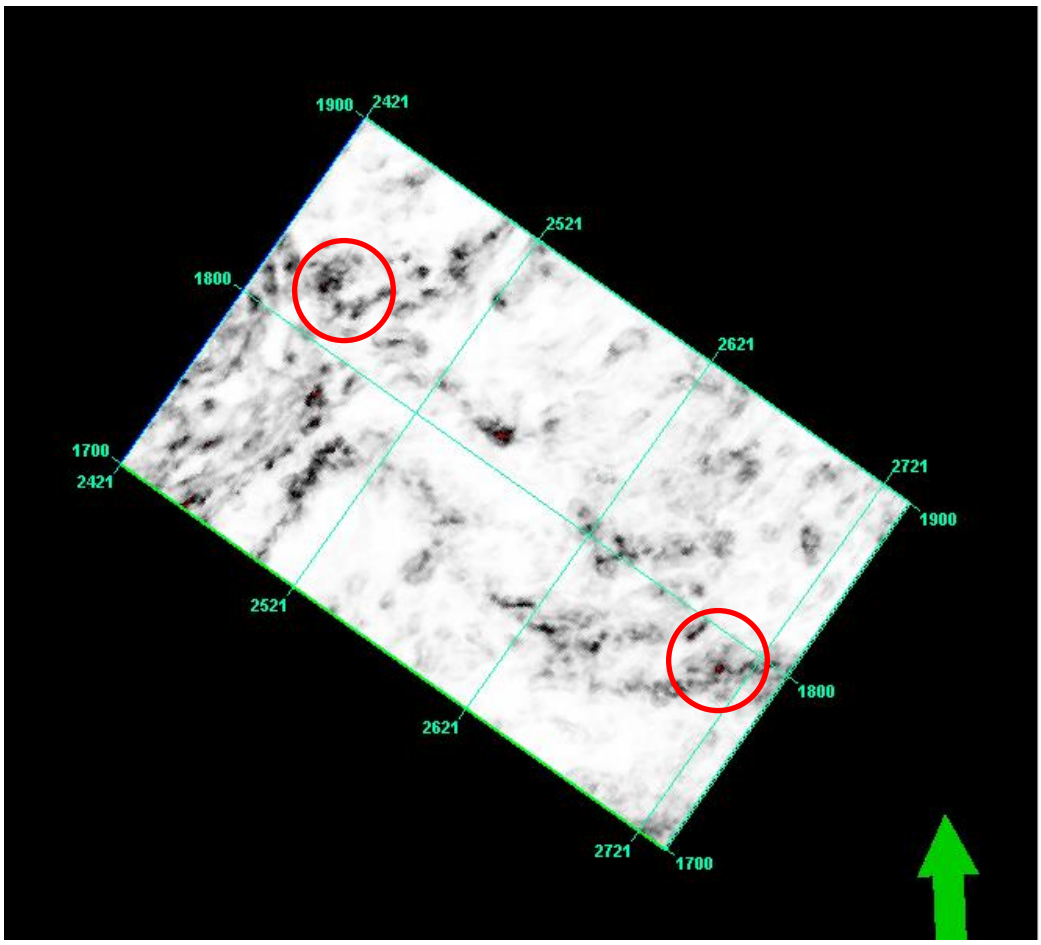

Figure 3.3 – Subvolume A Variance at 4000ms, 2x2, with dip correction.

In subvolume B, we apply the same parameters and find similar results. The shallow, regional faulting and minor fault dispersion are shown well, as seen in Figure 3.4. In this volume, we also observe the effects of not correcting for dip. As seen in Figure 3.4 the comparison between the variance volumes with dip correction (left) and without dip correction (right) shows that correcting for dip before calculating the variance reduces the

artifacts due to geologic structure. Though it should be noted that both calculations are accurate in the sense that true variance is shown – in both volumes, areas of high variance/low coherence do exist – but for the purposes of fault/fracture delineation, muting the areas with strong-dipping structure via dip calculation leaves only the areas where variance reflects the discontinuities due to faults (Figure 3.4, left). The variance calculation applied through all 3 subvolumes shows that the variance computation in Petrel, with adjusted spatial aperture and dip correction, is an accurate depiction of fault trending and fracture delineation.

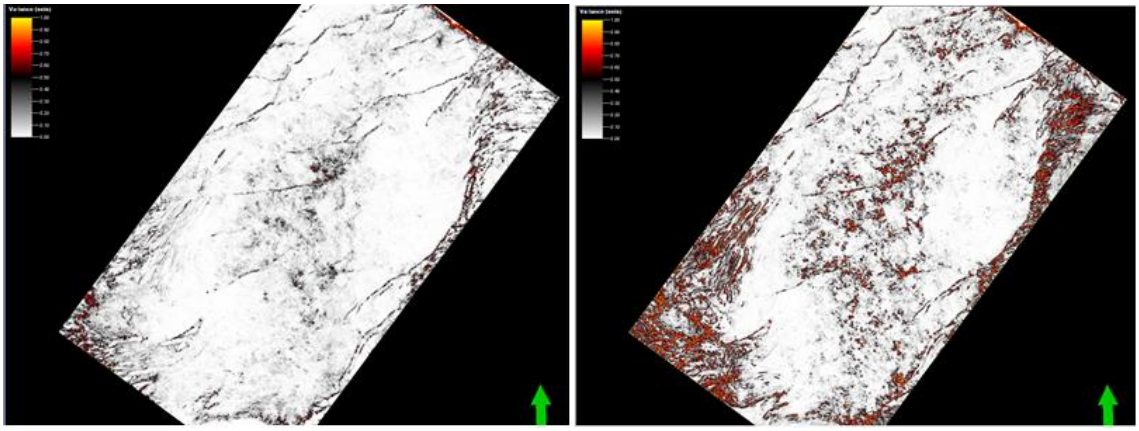

Figure 3.4 – Effects of calculating variance with (left) and without dip-scan (right). Note presence of artifacts in the variance due to structure in the variance volume on right.

Ant-tracking

Upon finding the optimal parameters for the variance calculation in the production zone, we apply the ant-tracking algorithm in attempt to depict the fracture network resulting from the faulting in the area. The ant-tracking algorithm and workflow are detailed in Figure

3.5.

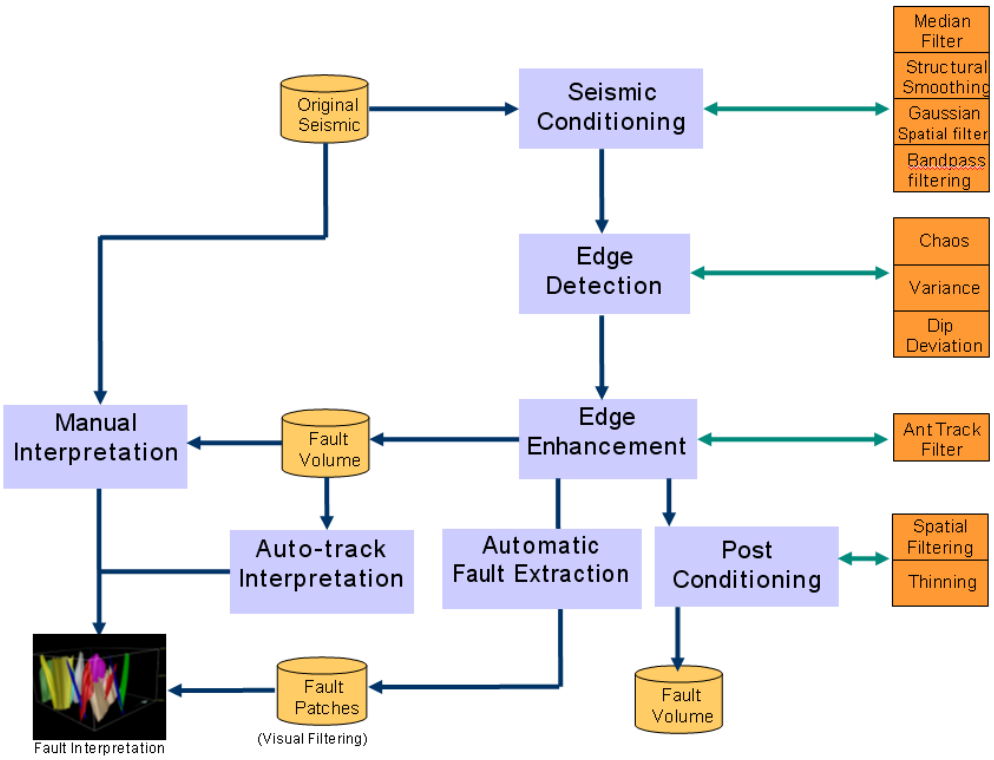

Figure 3.5 – Ant Tracking Algorithm (Petrel)

As described, we first condition a seismic cube with structural smoothing and edge enhancement to bring out the discontinuities in the data. The next step in the ant-tracking workflow is to run variance calculation on the edge-enhanced volume, which we completed with the parameters we found to be optimal. Using this edge-enhanced, variance volume as input to the ant-tracking algorithm, we obtain two different ant-tracking results. The first, shown in the left side of Figure 3.6 is the result of aggressive ant tracking parameters, which

attempts to make more 'connections' from the variance volume to describe the smaller fractures through the volume. The second ant-tracking option uses the passive parameters, which makes fewer connections through the variance volume, resulting in a depiction of the larger faults through the volume (Figure 3.6, right).

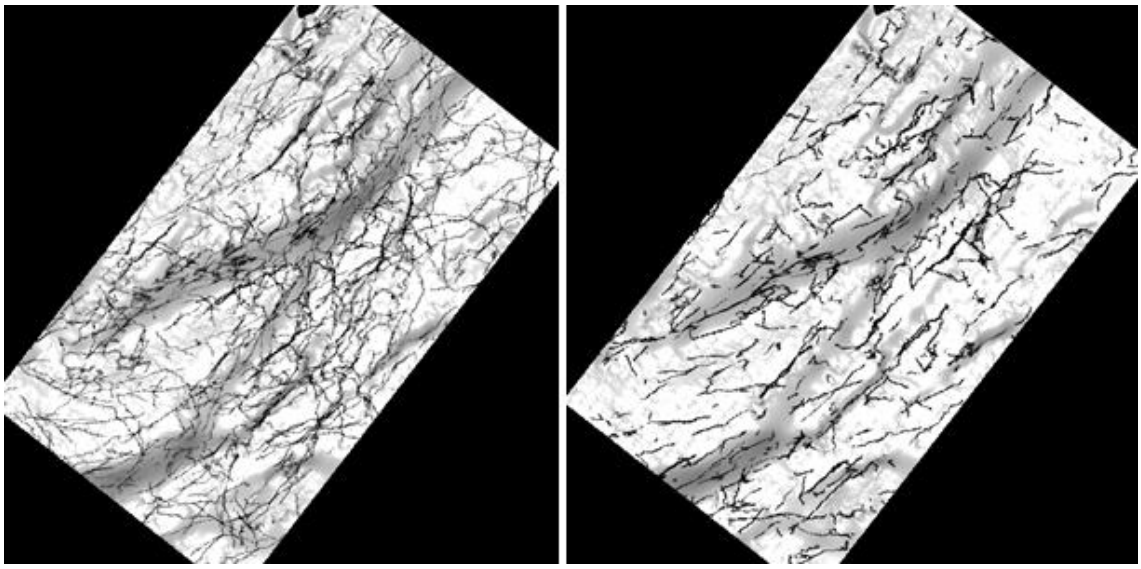

Figure 3.6 – Ant-tracking comparison, production area, along reservoir top horizon, from variance volume generated using a 2x2 spatial aperture, dip correction, and vertical smoothing factor of 47. Left image shows results of aggressive ant-tracking, where the tracker attempts to make more connections than the passive tracking on the right.

Eigenstructure Coherence

Eigenstructure coherence, as we recall, is advantageous due to the separation of waveform and amplitude into independent mathematical measures. We test eigenstructure coherence through our dataset via an 8-trace method in Landmark. We designate the coherence estimation to be completed along the top reservoir horizon and select a temporal analysis window of 40ms. The resulting eigenstructure coherence image is the most accurate

and detailed of the coherence techniques explored thus far for the low resolution dataset, showing the regional faults as well as fracture networks resulting from them in more detail than the 3-trace cross-correlation method, and less resolution loss compared to the variance computation in Petrel (Figure 3.7).

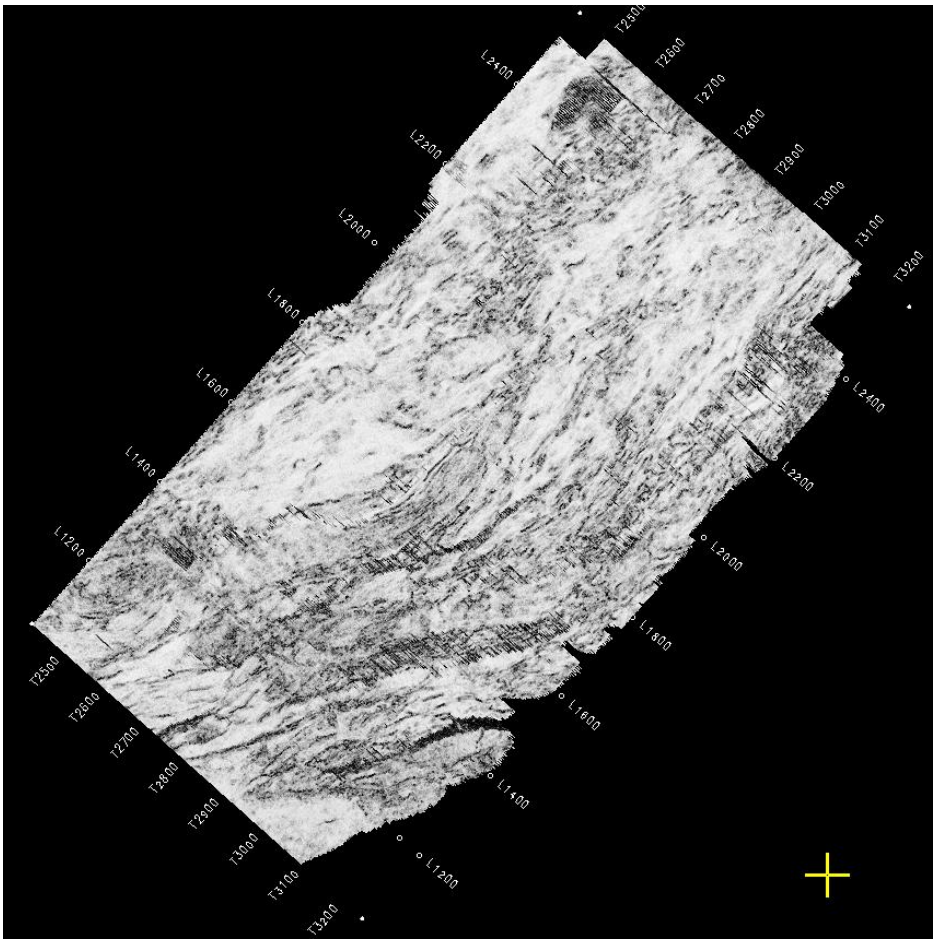

Figure 3.7 – 8-trace eigenstructure coherence estimate along temporal window of 40ms, low resolution

Curvature

Curvature, as previously mentioned, is a powerful tool in enhancing the visibility of fracture zones, thereby aiding coherency methods in fault/fracture determination. In our study of the low-resolution dataset, we use Landmark software to calculate and compare two methods of curvature – Gaussian and most positive/negative curvature. In Landmark, we have the option available to calculate curvature through volumes defined by horizons: time windows +/- a user-defined number of milliseconds above and below the horizon. This allows for much faster calculation time, which enables us to bypass the sub-volume cropping and evaluate curvature for the entire dataset.

We find that most-positive and most-negative curvature yield the best results in determining faults and fractures. This is due to the observation that most-positive/negative curvature values are the same polarity for a given geologic feature. Gaussian curvature, on the other hand, tends to yield values of zero for geologic features such as valleys or ridges with non-zero curvature in one direction. This is reasonable due to the fact that k_{min} values are around zero for these features, which can be indicative of faulting, and due to the calculation of Gaussian curvature as detailed previously, when k_{min} values fluctuate about zero, the Gaussian curvature also will be zero. Thus, Gaussian curvature is not as ideal for fault/fracture mapping as most-positive or most negative curvature.

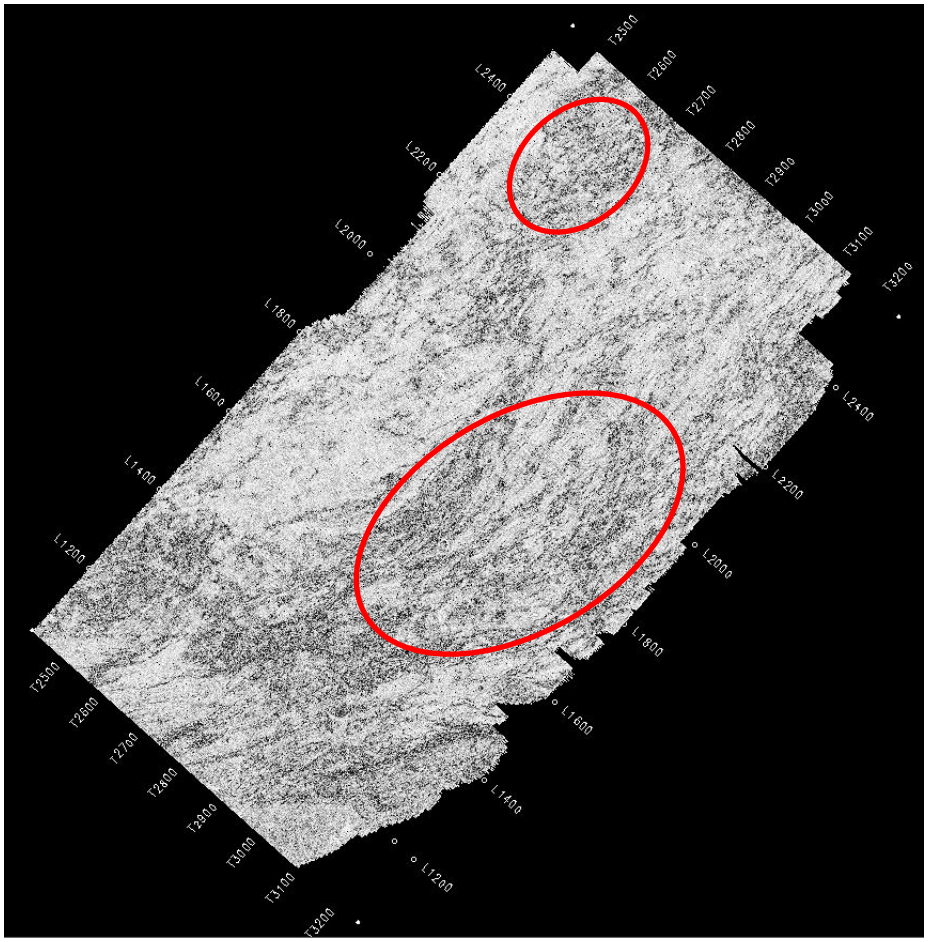

Figure 3.8 – Most Positive Curvature Low Resolution, temporal window 20ms

As can be seen in Figure 3.8, the most-positive curvature map effectively identifies general fault trends as well as the areas with high fracture density (red circles). When compared to the variance subvolumes from Petrel and the eigenstructure volume in Landmark, we find that the volumetric curvature calculation for most-positive curvature shows the most minor fault detail. We also note, however, that the most-positive curvature loses major fault detail as a tradeoff.

Conclusions

From the attribute analysis and parameter testing in the low-resolution dataset, we find that for general fault trend mapping, 8x8-trace eigenstructure coherence along a temporal aperture of 40ms is the optimal analysis method. For identifying minor faulting around these major faults and predicting fracture networks around these areas, the most-positive curvature method using a spatial aperture of 3x3 traces and a temporal window of 20ms is the preferred method. A tradeoff in the most-positive curvature results is seen in the decreased resolution of the major faults at the Reservoir Top horizon level. It is our expectation that these two methods will also be the best attributes for depicting general and minor faulting in the high resolution volume as well, though the parameters for each are likely to require adjusting.

CHAPTER IV

HIGH RESOLUTION (60Hz) DATASET ATTRIBUTE ANALYSIS

Introduction

In this chapter, we apply the findings from our investigation in the low-resolution (15 Hz) dataset to the coherence and curvature analysis in the high-resolution data (60 Hz). From interpretation of the high-resolution data, we observe the differences from the original dataset in higher density of faults and fractures visible on seismic. Thus, we can proceed to apply the coherence and curvature algorithms to the high resolution dataset to compare with the results we obtained previously from the low-resolution dataset. A further step we take with the high-resolution dataset is the analysis of most-positive curvature results with P-wave impedance inversion results generated by Zhang et al. (2014) for identification of zones through the reservoir most likely to contain fractures.

Data Interpretation and Conditioning

As the high resolution dataset at 60 Hz is twice the size of the low resolution dataset, our subvolume cropping is again required for calculation of variance in Petrel. We apply the same structural smoothing with edge-enhancement to the cropped volumes to enhance the discontinuities in the reflectors.

Coherence Parameter Testing

We use Petrel to estimate coherence using the variance method previously mentioned. As with the lower resolution volume, test the parameters for Petrel's variance algorithm for each subvolume, then test the parameters for cross-correlation and

eigenstructure coherence in Landmark. In doing so, we are able to visualize the effects of altering the aperture window size and analysis time window on seismic data, and observe if any of these effects changed due to the increased resolution of seismic data.

Results

Variance

We apply the same variance parameters we determined to be optimal in delineating faults and fractures in the low resolution dataset to our 60 Hz dataset. We find that the variance calculation, again, accurately shows the areas of low coherence and, with dip correction, most of these high variance zones are due to faulting or fracture density. This is seen in our production sub-volume C, though it must be noted, that the high resolution data variance images still suffer from loss of image clarity from zooming in (Figure 4.1).

We confirm that the variance calculation reflects the increased fracturing resulting from the increased resolution of seismic data by testing the variance of high-resolution subvolume B. In Figure 4.2 we observe the differences between the low and high resolution variance volumes, indicating the areas of increased fractures due to the high resolution volume (circle) and confirming that the variance algorithm is able to identify these zones.

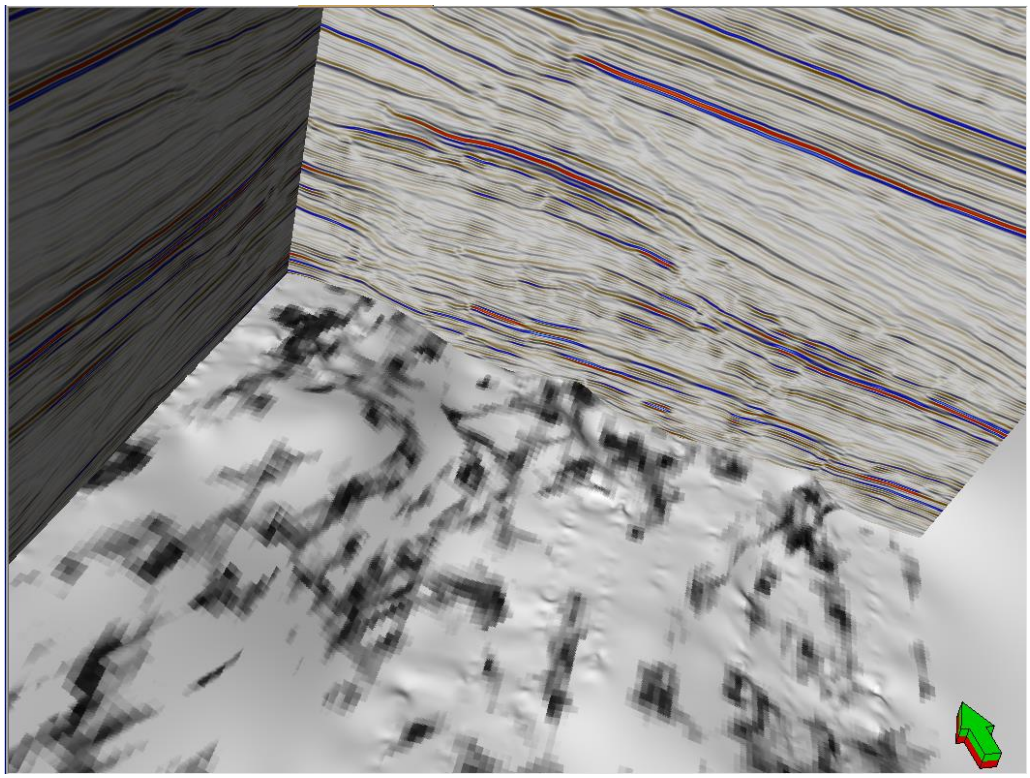

Figure 4.1 – High Resolution Variance at Reservoir Top

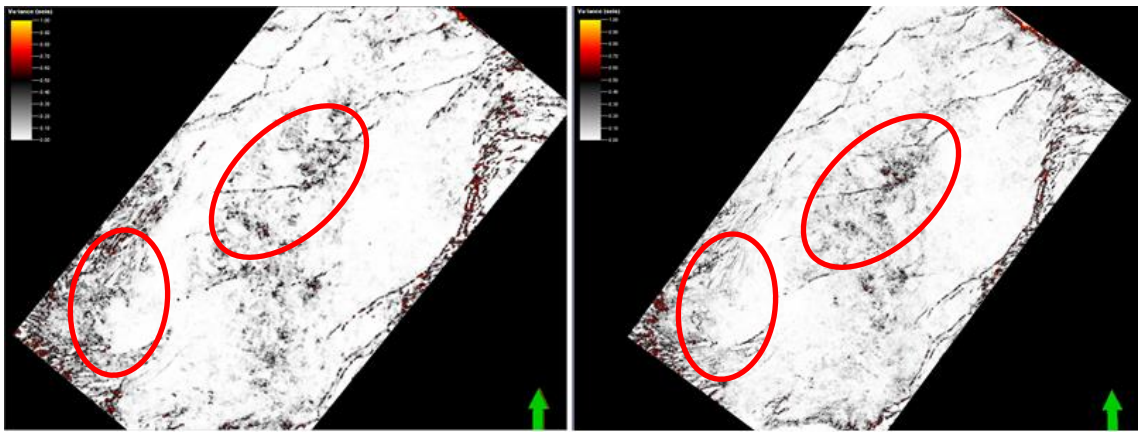

Figure 4.2 – Variance at 1050ms for (left) low resolution and (right) high resolution dataset

Ant-tracking

Figure 4.3 shows the results of applying ant-tracking to the variance cubes from subvolume C in the high resolution dataset. The results of passive ant-tracking is shown on the left and aggressive-parameter ant-tracking is displayed on the right. Again, we observe that, due to the increased resolution in seismic, we obtain more variance values in the areas where discontinuities are present, and therefore more connections made by ant-tracking. Also, the aggressive-parameter ant-tracking does make more connections than the passive, as described in Petrel. We find, however, that ant-tracking in the high-resolution dataset becomes increasingly interpreter-influenced, as we are forced to apply passive parameters regardless of intent to map large-scale faults or detailed fracture networks, as the increased detail from the high resolution seismic creates too many connections for ant-tracking regardless of the parameters set.

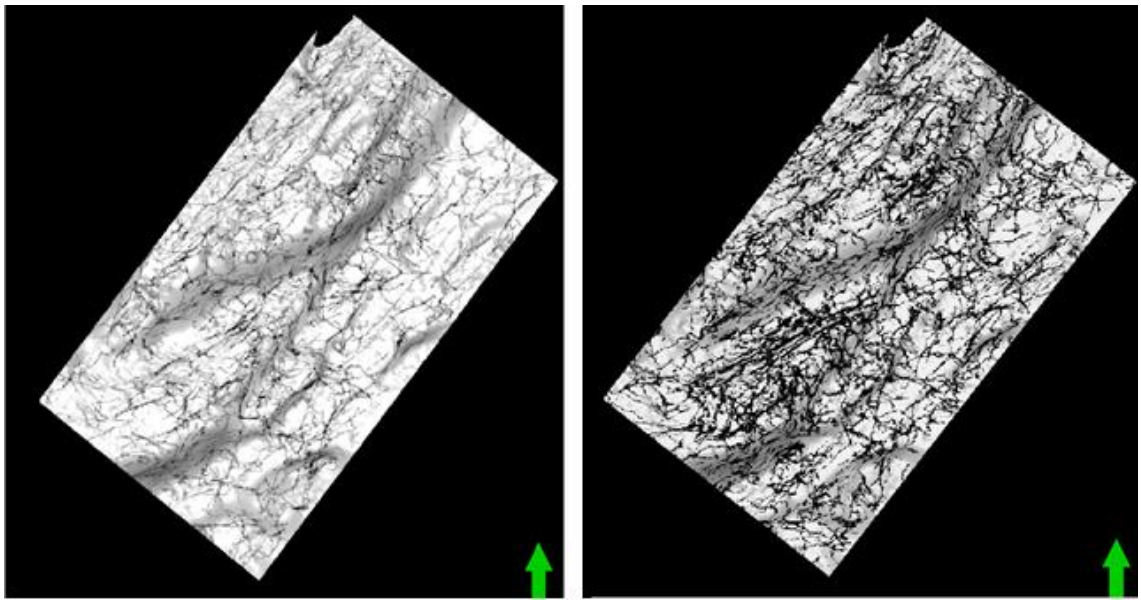

Figure 4.3 – Ant tracking passive (left) and aggressive (right) parameters for high resolution data

Eigenstructure-based Coherence

Eigenstructure coherence is calculated with an 8-trace method in Landmark. We designate the coherence estimation to be completed along the top reservoir horizon and select a temporal analysis window of 40ms. The resulting eigenstructure coherence image is the most accurate and detailed of the coherence techniques explored thus far for the high resolution dataset, showing the regional faults as well as fracture networks resulting from them in more detail than the 3-trace cross-correlation method, and less resolution loss compared to the variance computation in Petrel (Figure 4.4).

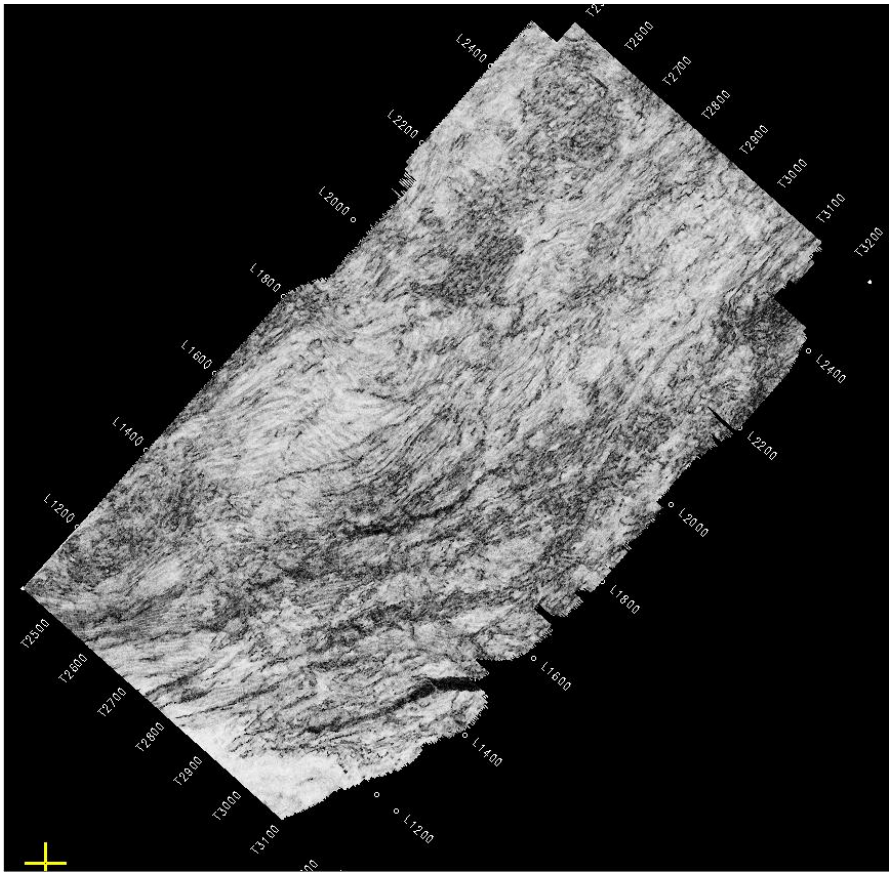

Figure 4.4 – 8 trace eigenstructure coherence from Top Reservoir horizon for high resolution dataset

Curvature

In our analysis of the low-resolution dataset, we determined that most-positive and most-negative curvature calculations were superior to Gaussian curvature for describing faults and fractures. Therefore, we apply the most-positive curvature algorithm to the high resolution dataset in Landmark. Though the dataset is twice as large, we are still able to calculate the curvature from a narrow window of traces above and below Reservoir Top horizon, then extract the curvature values to the Reservoir Top horizon for display. The most-positive curvature generated from the high resolution seismic is compared to the previous curvature map from the low-resolution data, and we can observe the increased detail in Figure 4.5 with the areas of higher fracture density circled (red). It is observed that the south and central-eastern region of the field shows the most small fault activity, with fracture density dispersed through that area and around the major faults.

Also, when compared to the high-resolution variance subvolumes from Petrel and the high resolution eigenstructure volume in Landmark, we find that the volumetric curvature calculation for most-positive curvature shows more minor fracture detail and is thus most useful when used together with eigenstructure coherence. As observed in Figure 4.6, when we compare the high resolution coherence and curvature volumes side-by-side, we observe large fault zones in the coherence volume but more minor fault detail in the curvature (red square). Both attributes are taken from Top Reservoir horizon.

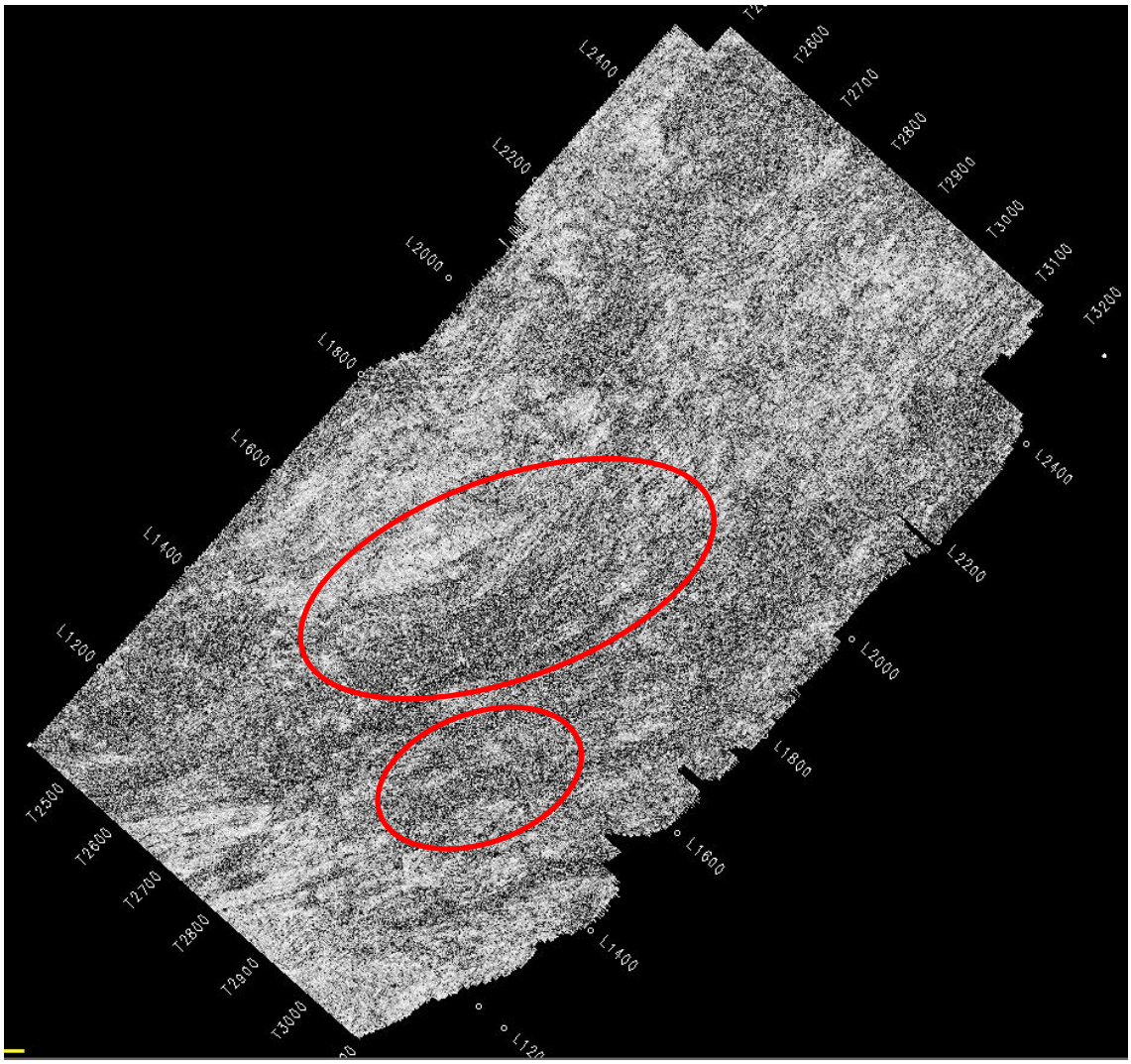

Figure 4.5 – Curvature values from Top Reservoir horizon, high resolution dataset

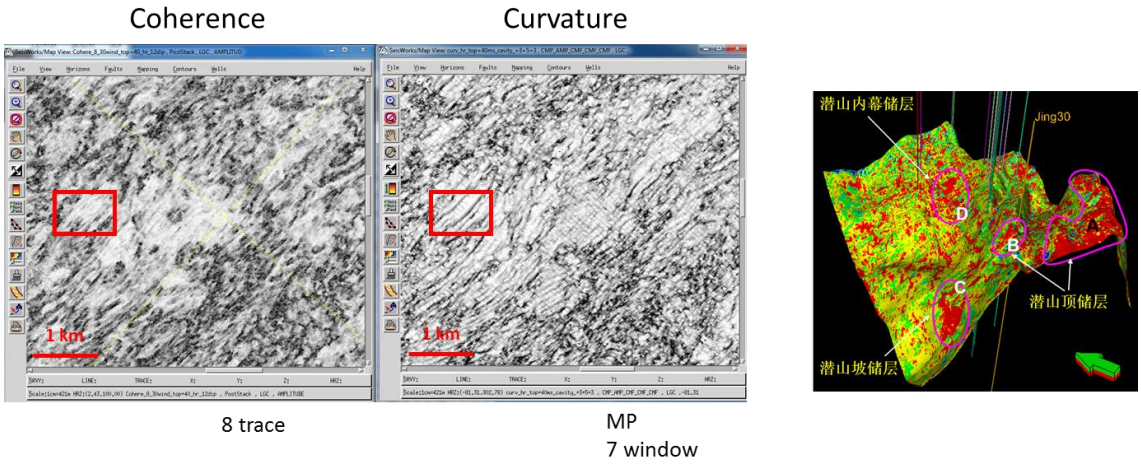

Figure 4.6 – High-resolution coherence volume (left) and high resolution curvature volume with increased minor fault detail (middle). Image on right shows the region from Top Reservoir horizon the two attribute maps depict (Zhang et al., 2014)

Comparisons Between Low-resolution and High-resolution

From parameter testing, we observe that applying different parameters for spatial/temporal aperture, as well as accounting for dip correction, can alter the results of the attribute analysis significantly. We also note, however, that adjusting these values can bring out or mute some features, and it is largely up to the interpreter to decide which features are of more interest and apply the appropriate attribute analysis and parameters. From Figure 4.7a and b, we observe the differences between eigenstructure coherence and most-positive curvature using 3 different sets of parameters. It is observed that generally, the high resolution data and attribute volumes (Figure 4.7b) show more detail, with different features accentuated depending on the parameters chosen. However, we also observe the low-resolution coherence volume (top left, Figure 4.7a) to be a better depiction of the general and minor faulting in the zone of study than the corresponding high-resolution coherence (top

left, Figure 4.7b). This is due to smearing of the coherence values due to the increased resolution of seismic data in the 60Hz volume. All attribute maps are generated from and extracted to the Reservoir Top horizon.

Comparing the attribute results from the two datasets, we observe a greater amount of fault detail in the high resolution coherence and curvature volumes. This is largely due to the increased seismic resolution in the 60Hz volume. A comparison of the eigenstructure coherence and most-positive curvature methods for the low and high-resolution data is shown in Figure 4.8a and b, with areas of increased minor fault detail indicated by red boxes.

This increased attribute resolution must be confirmed by interpretation to the high resolution seismic data volume to affirm the minor faulting observed on the curvature horizons are reliable, and not due to artifacts.

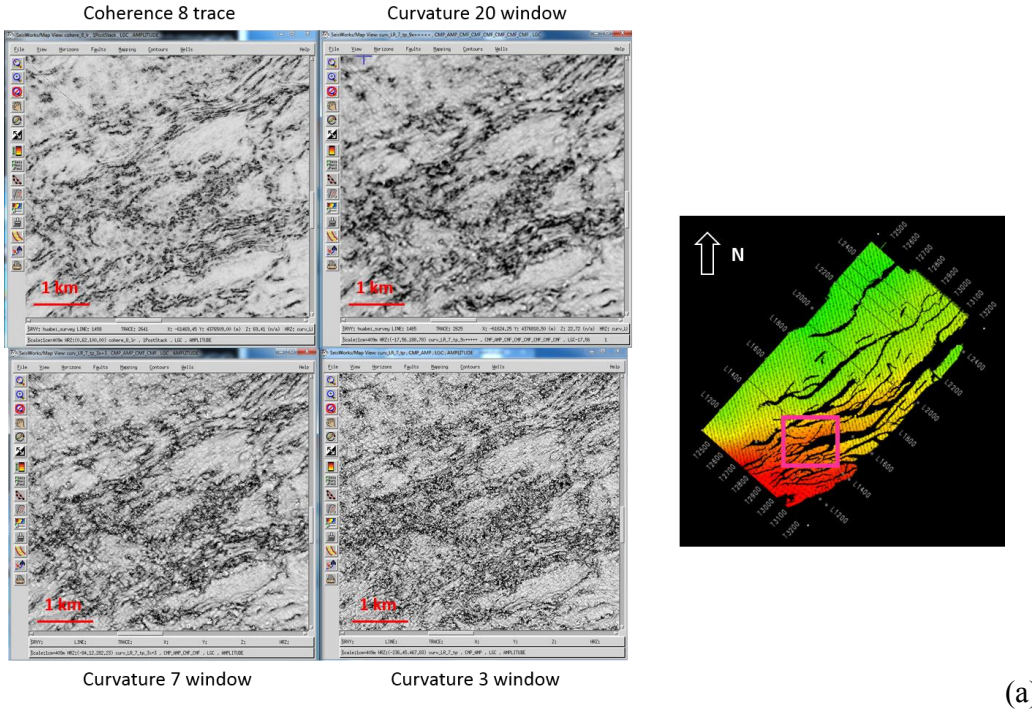

Figure 4.7 – Comparison of eigenstructure coherence and parameter testing for most-positive curvature in the low resolution data (a) and high resolution (b).

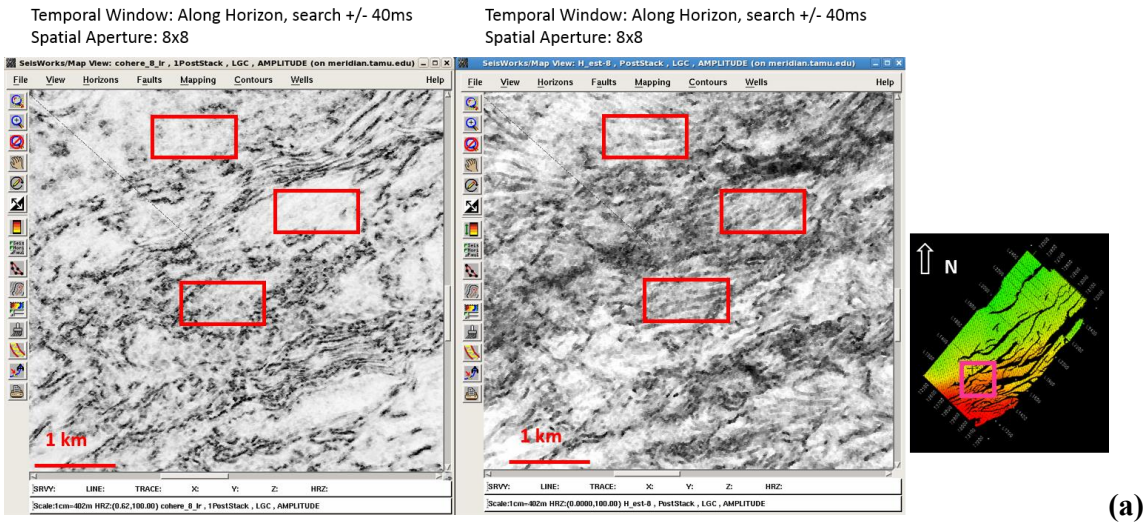

Figure 4.8 – Comparison between attribute analyses results between low resolution (left) and high resolution (right) for eigenstructure coherence (a) and most-positive curvature (b)

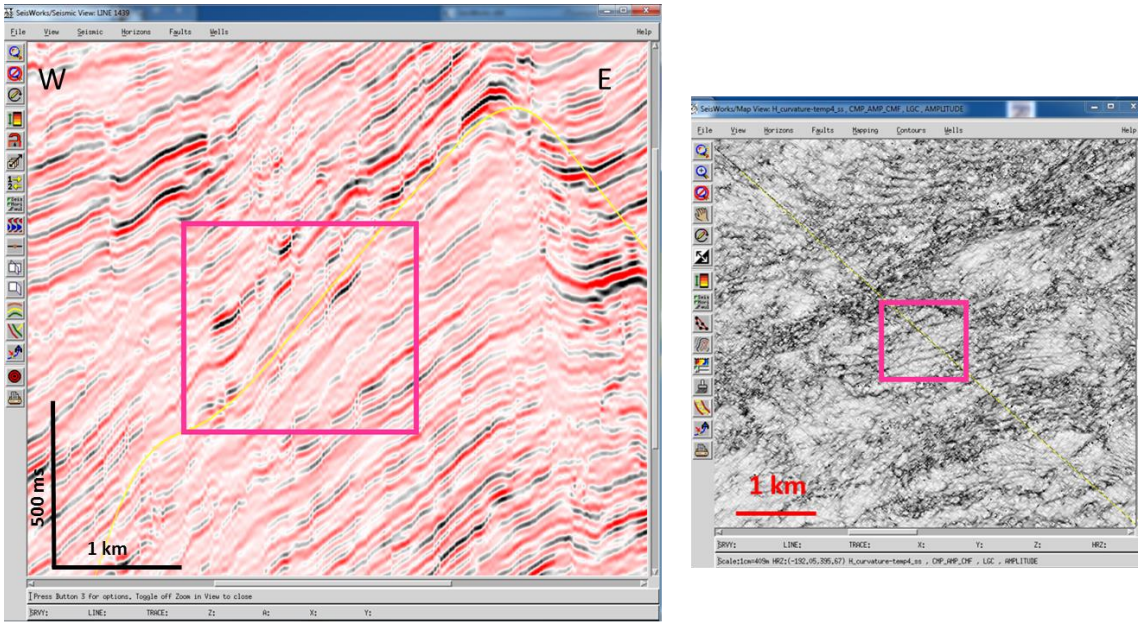

Figure 4.9 – Seismic interpretation of inline 1439 for confirming the increased minor fault detail from most-positive curvature (right) is due to evidence of faulting from the increased resolution from the high-resolution data (left)

This interpretation is show in Figure 4.9 and 4.10, where we compare inline 1439 from the high-resolution dataset to the intersection on the curvature horizon. From the interpretation, it is confirmed that there is clearly seismic evidence for the increased minor fault resolution on the calculated most-positive curvature horizons.

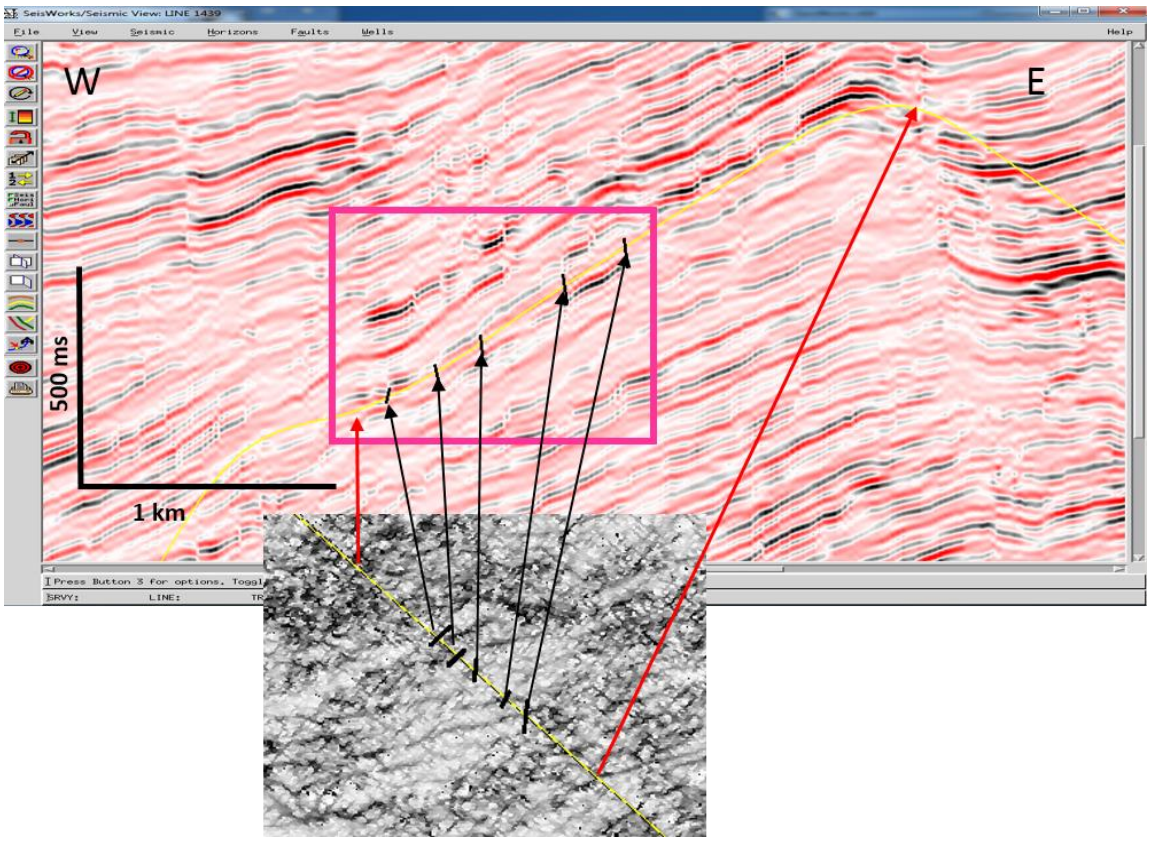

Figure 4.10 – Interpretation of inline 1439 to corresponding curvature attribute map intersection at Reservoir Top horizon (yellow horizon). Larger fault in region is shown on the most-positive curvature horizon (red arrow)

Comparing Most-positive Curvature Horizons to Low-impedance Zones

With our finding the most-positive curvature obtained from the high resolution dataset to be the most accurate attribute description of minor faulting and possible fracture zones, and having confirmed, via interpretation, the existence of the minor faults observed from the curvature horizons, the next step in our investigation is to compare the curvature horizons to P-wave impedance horizon slices generated from well log data inversion.

Zhang et al. (2014) generated horizon slices from Top Reservoir depth to +140ms deep, in 5ms intervals, extracting impedance values obtained through well log P-wave

velocity inversion. Due to the rock properties which determine impedance – velocity, density – low impedance zones can indicate areas in the rock contains fractures. In a carbonate reservoir such as the one of interest in our Huabei field study, fractures induce high porosity and permeability zones, which are strong hydrocarbon indicators. As previously stated, from exploratory wells drilled in the region hydrocarbon shows are present and suggest a potential producing reservoir.

From Zhang's impedance inversion analysis, and with an understanding of the burial history and geology of the region, we identify several zones at varying depths in the reservoir where low impedance is likely due to fractures in the carbonate rock. At these depths and areas, we generate the corresponding most-positive curvature horizon attribute for comparison and validation that these low impedance values are indeed indicators of fracture-heavy zones in the reservoir.

One such low-impedance zone that Zhang et al. (2014) identified is defined by the Reservoir Top horizon depth, at the intersections of inline 2110 and crossline 2970. We interpret the seismic line and crossline and determine the curvature-described minor faulting to be genuine (Figure 4.11a, b and 4.12). The red lines indicate the regional faulting and the green lines describe the smaller faults in the reservoir. The curvature horizon is then compared to the impedance horizon, and we observe that in this low impedance zone, there is indeed evidence of major and minor faulting pathways, around which fracture networks can be expected.

Line 2110 Most-Positive curvature

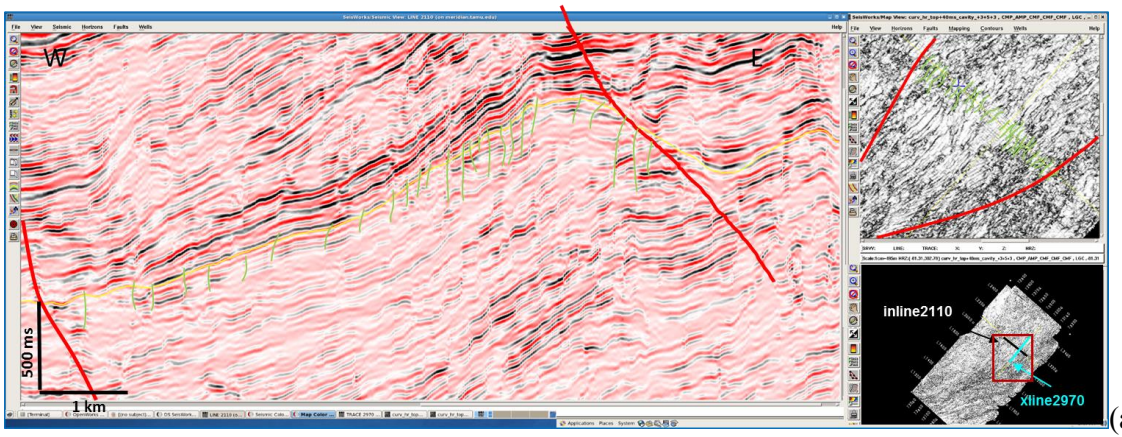

(a)

Xline 2970 Most-Positive curvature

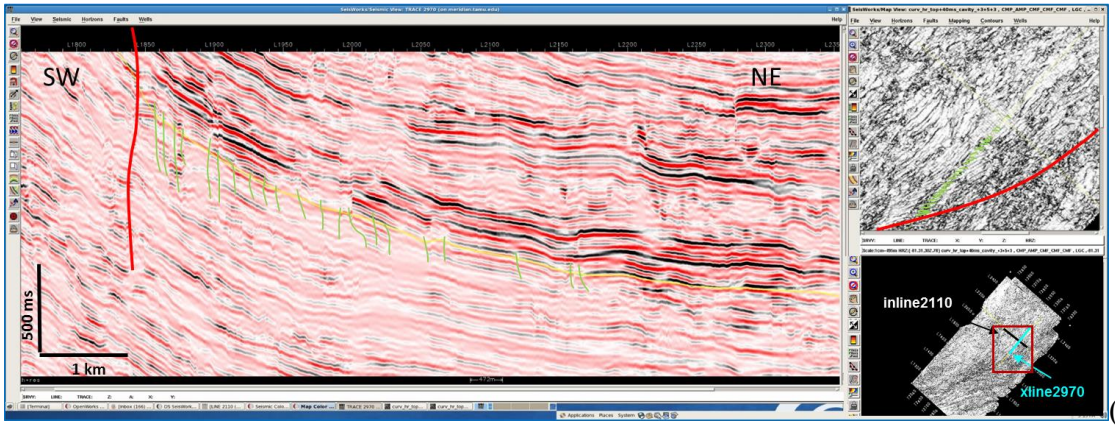

(b)

Figure 4.11 – Interpretation of inline 2110 (a) and crossline 2970 (b), which defines the low-impedance zone (Zhang 2014), to most-positive curvature at Top Horizon level. Green lines indicate the minor faulting, red lines indicate regional faults.

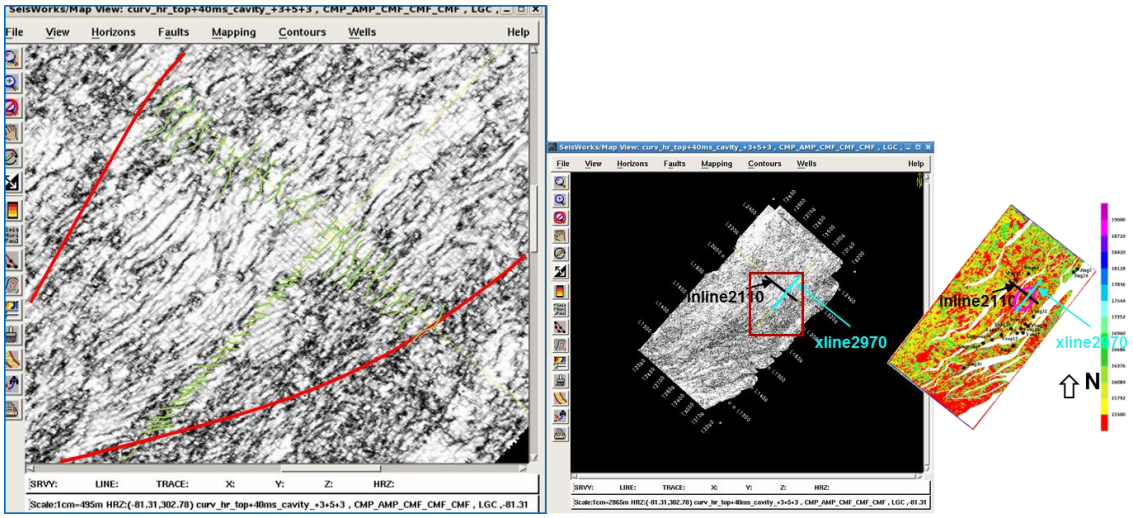

Figure 4.12 – Combined interpretation displayed on Top Reservoir depth most-positive curvature, showing that the low-impedance zone defined by Zhang (2014) has strong evidence of minor faulting and possible fractures.

The figures which follow (Figures 4.13-4.20) illustrate the same analysis performed at different zones of low impedance determined to be of prospective reservoir interest throughout the carbonate reservoir of Huabei field. These low impedance zones are not due to rapid changes in lithology or unconformities (Zhang 2014) and therefore we investigate each zone further by using the corresponding most-positive curvature attribute analysis at each horizon time slice.

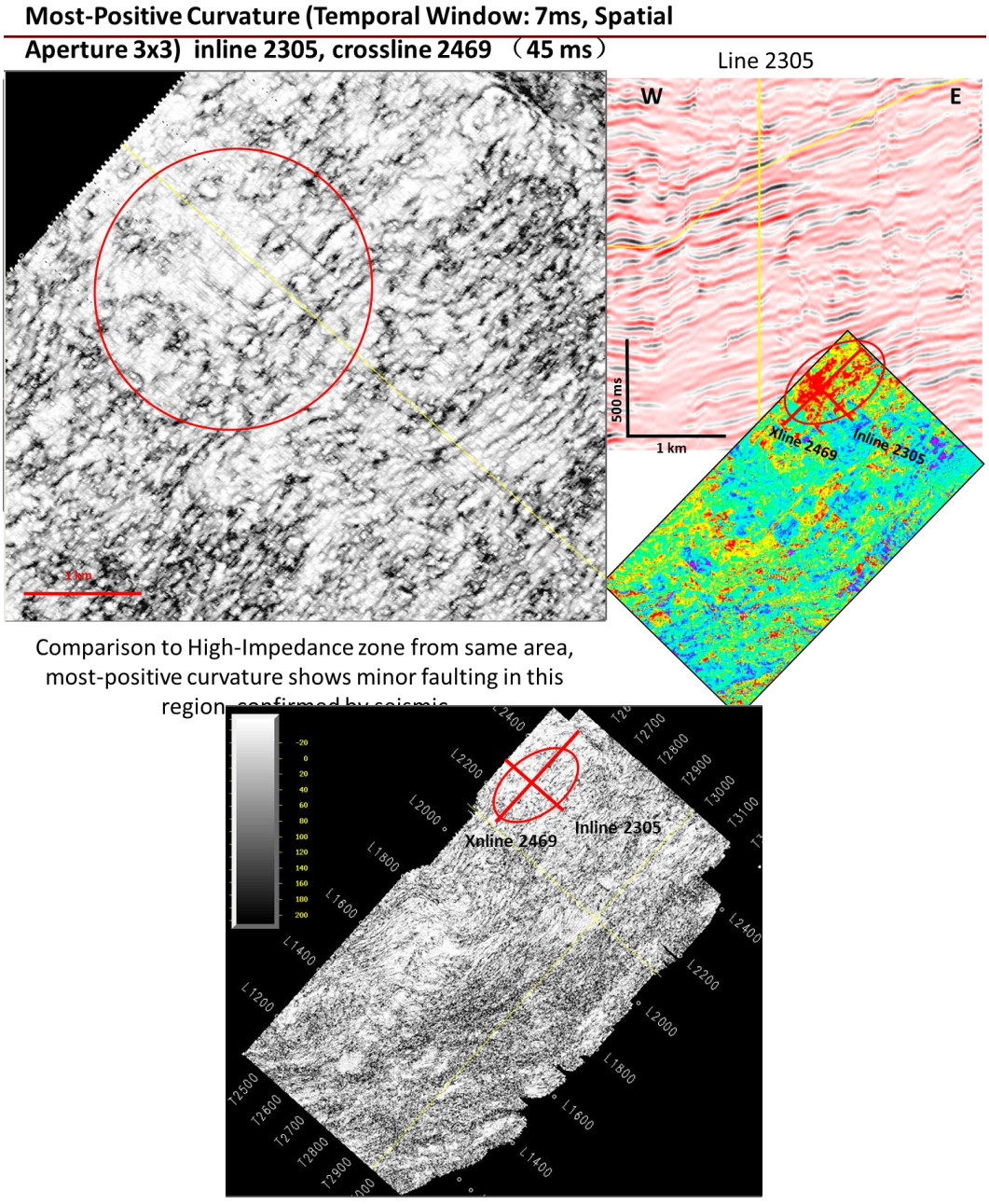

Figure 4.13 – Comparison of impedance and curvature horizon slices at 45ms, where a low-impedance zone is observed in the northwest region of the field. Interpretation from high-resolution dataset and most-positive curvature horizon confirms that there exists evidence of minor faults in the zone.

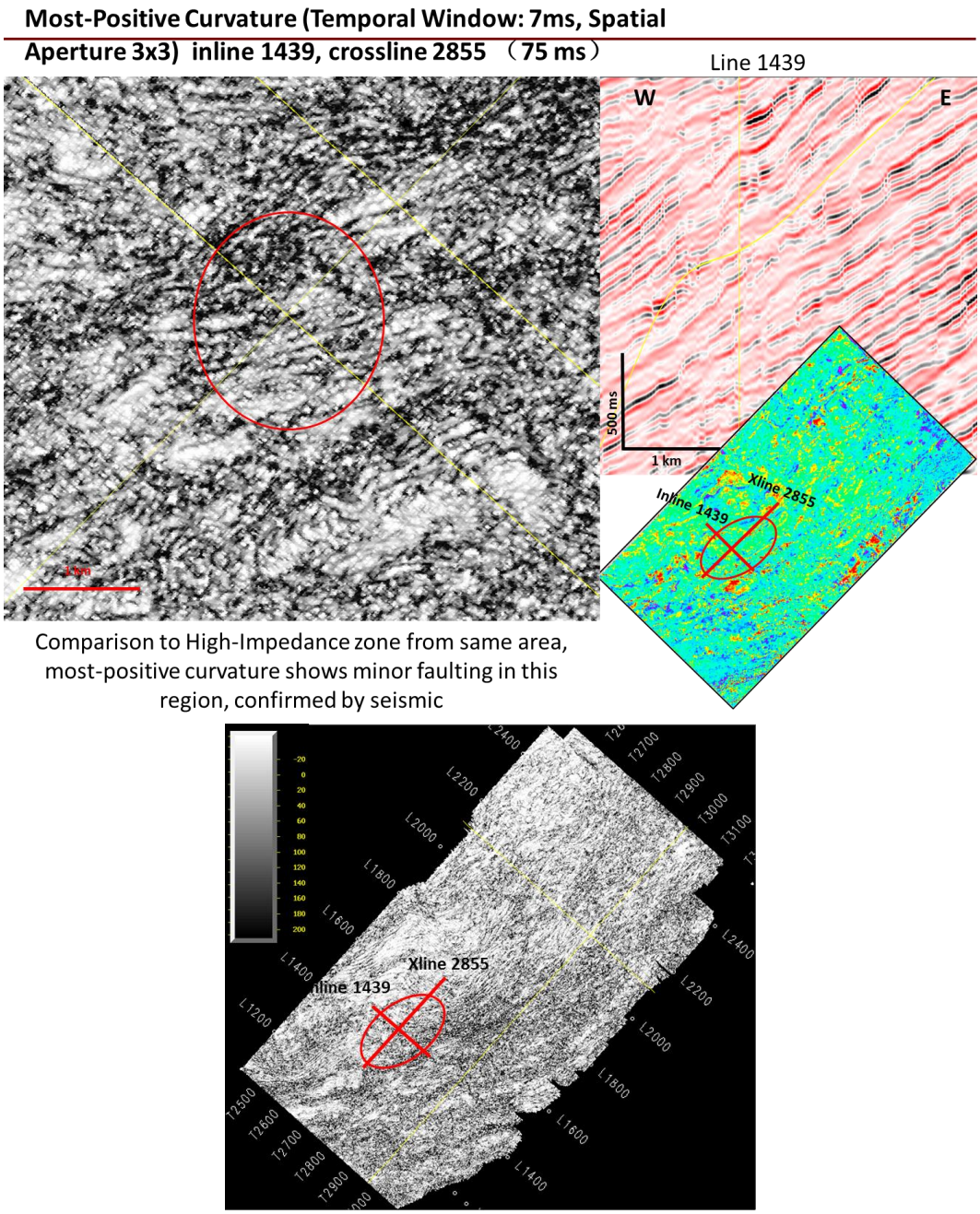

Figure 4.14 – Comparison of impedance and curvature horizon slices at 75ms, where a low-impedance zone is observed in the southwest. Interpretation from high-resolution dataset and most-positive curvature horizon confirms that there exists evidence of minor faults in the zone.

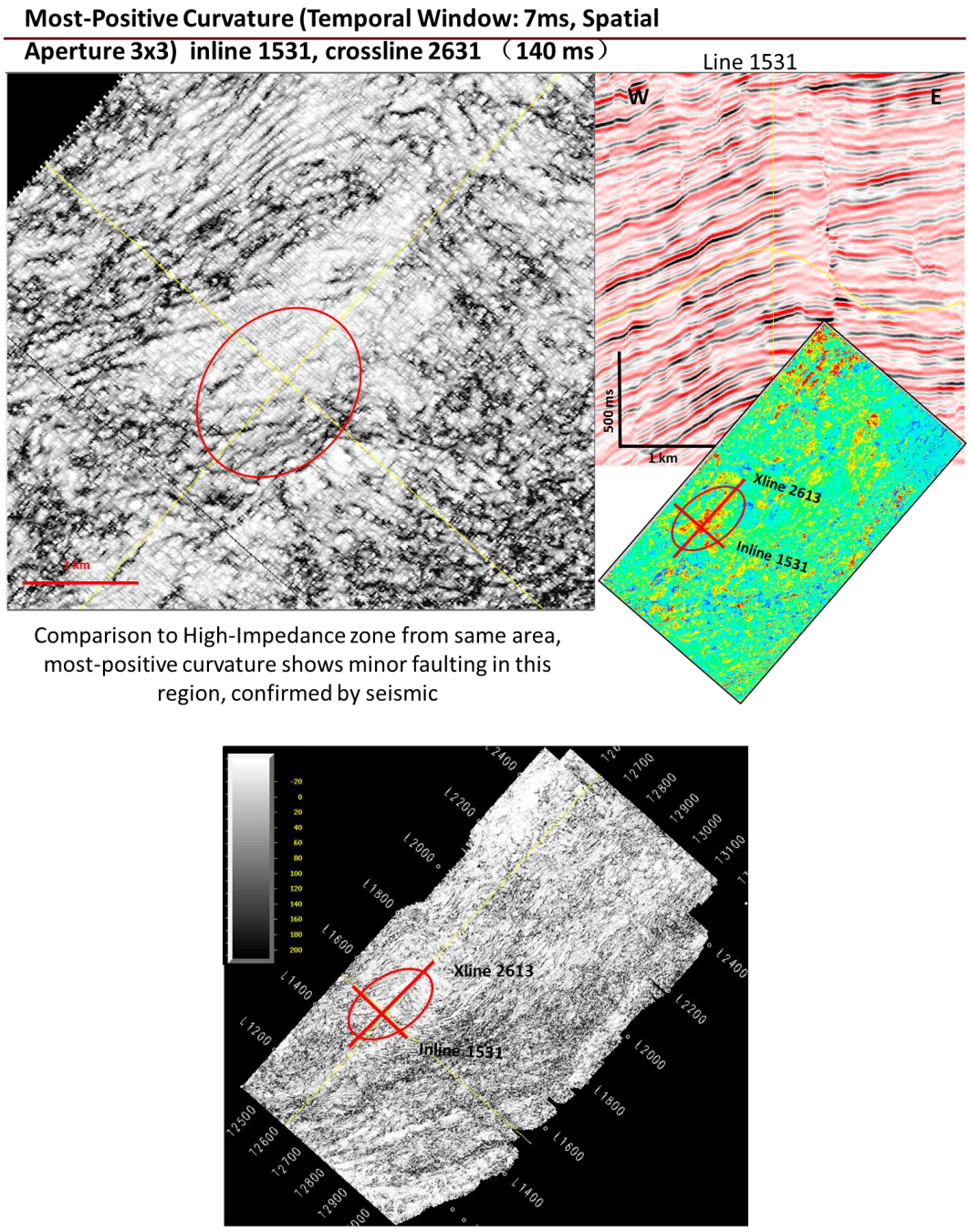

Figure 4.15 – Comparison of impedance and curvature horizon slices at 140ms, where a low-impedance zone is observed in the southwest. Interpretation from high-resolution dataset and most-positive curvature horizon confirms that there exists evidence of minor faults in the zone.

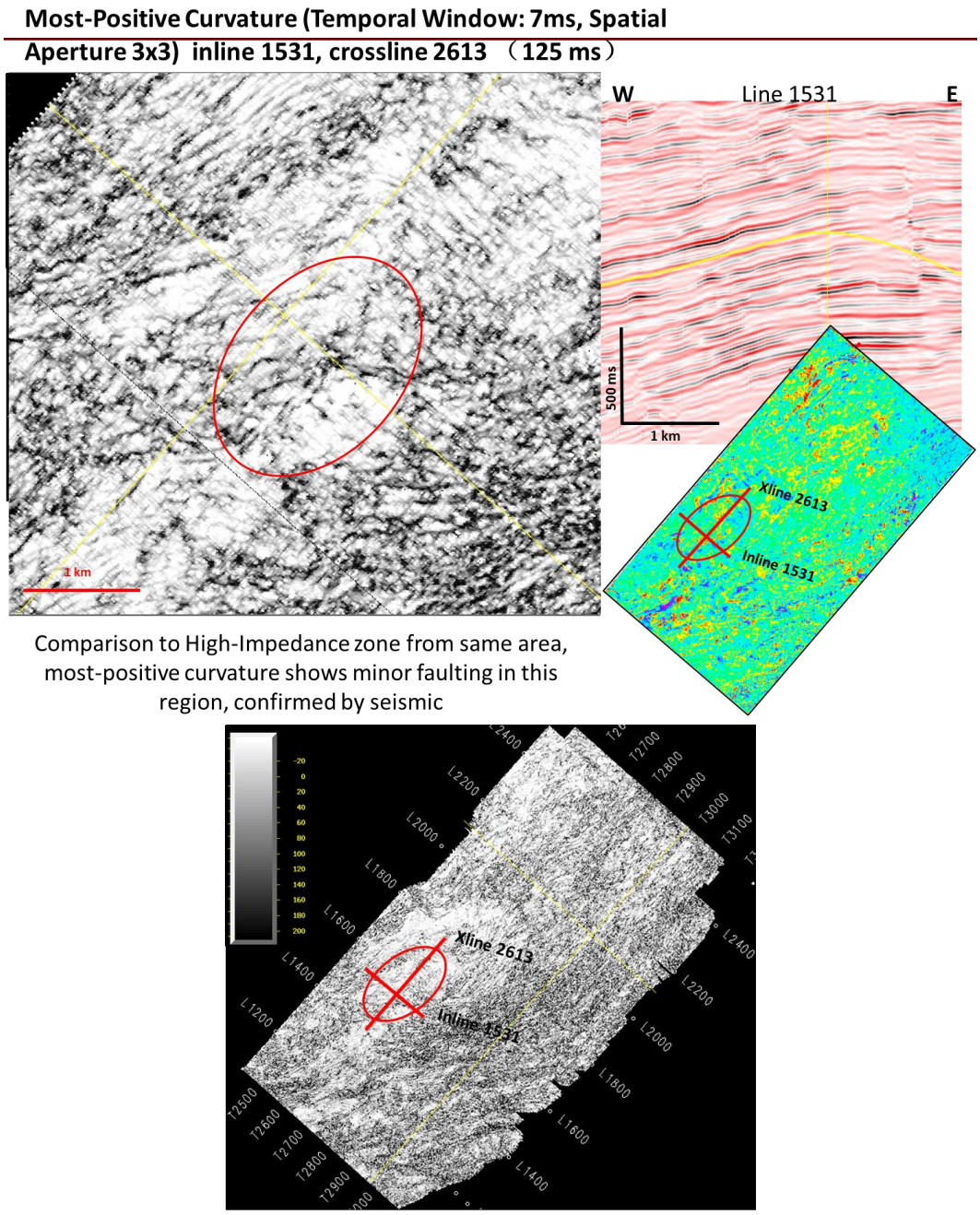

Figure 4.16 – Comparison of impedance and curvature horizon slices at 125ms, where a low-impedance zone is observed in the southwest. Interpretation from high-resolution dataset and most-positive curvature horizon confirms that there exists evidence of minor faults in the zone.

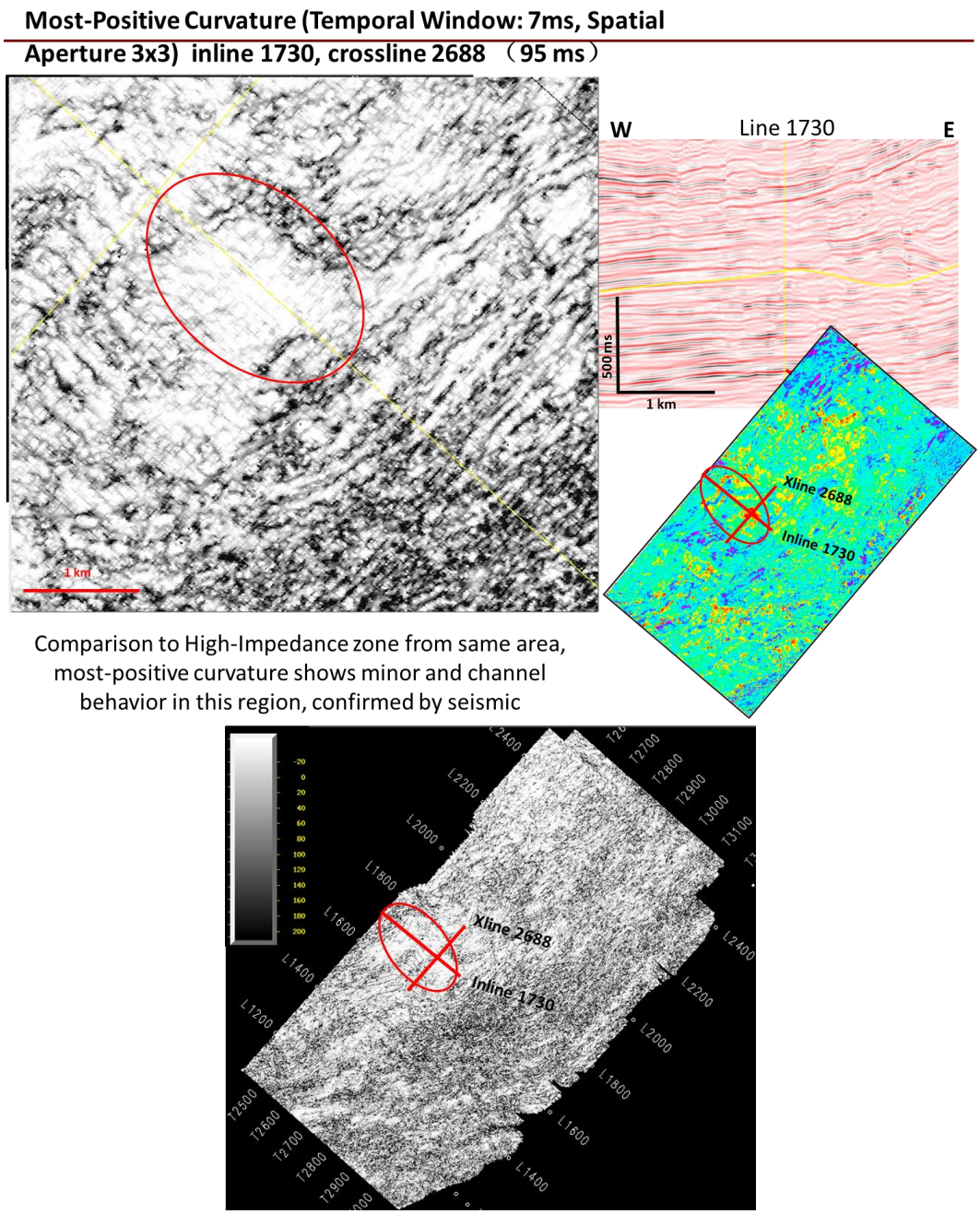

Figure 4.17 – Comparison of impedance and curvature horizon slices at 95ms, where a low-impedance zone is observed in the central-western zone. Interpretation from high-resolution dataset and most-positive curvature horizon confirms that there exists evidence of minor faults in the zone.

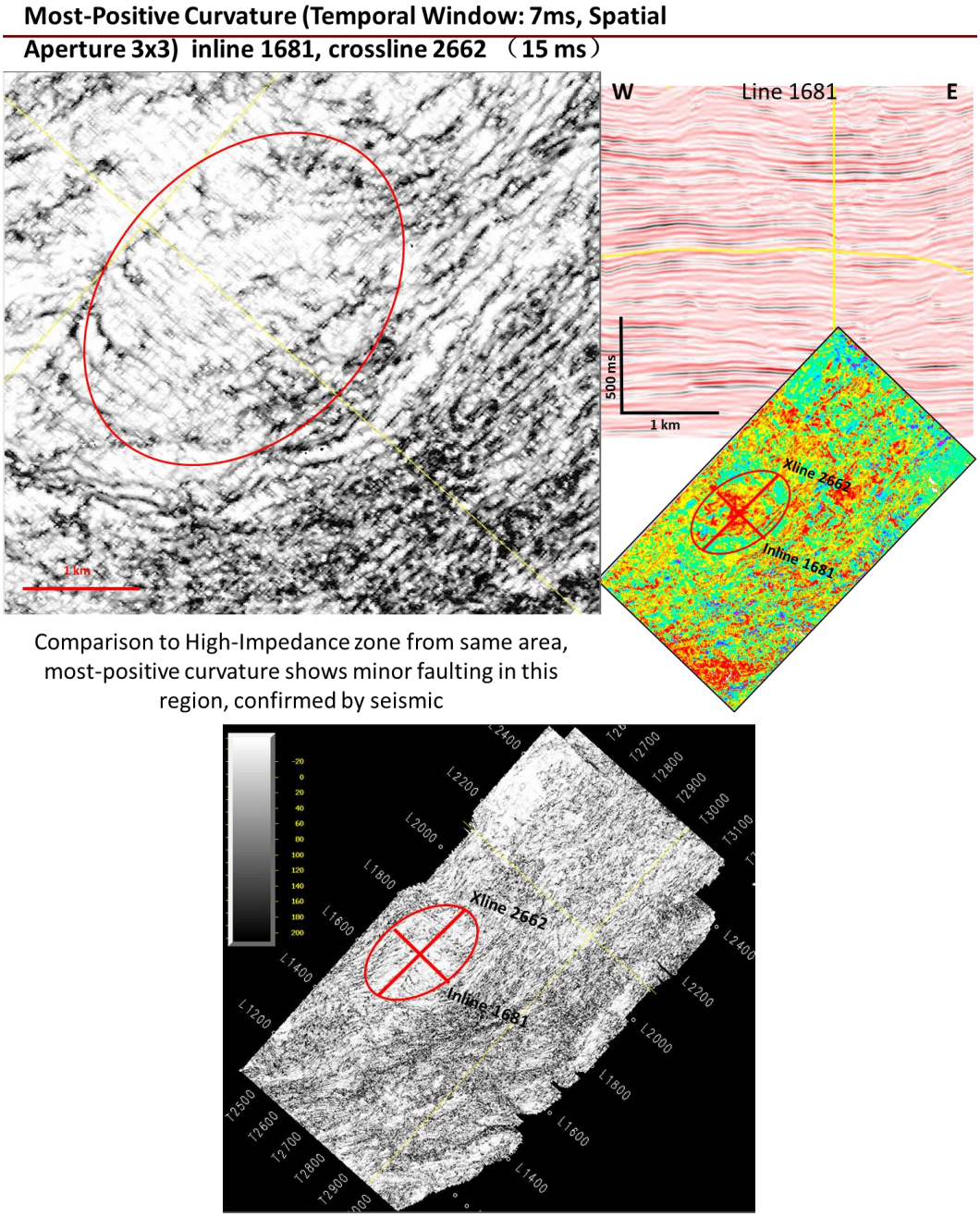

Figure 4.18 – Comparison of impedance and curvature horizon slices at 15ms, where a low-impedance zone is observed in the central-western zone. Interpretation from high-resolution dataset and most-positive curvature horizon confirms that there exists evidence of minor faults in the zone.

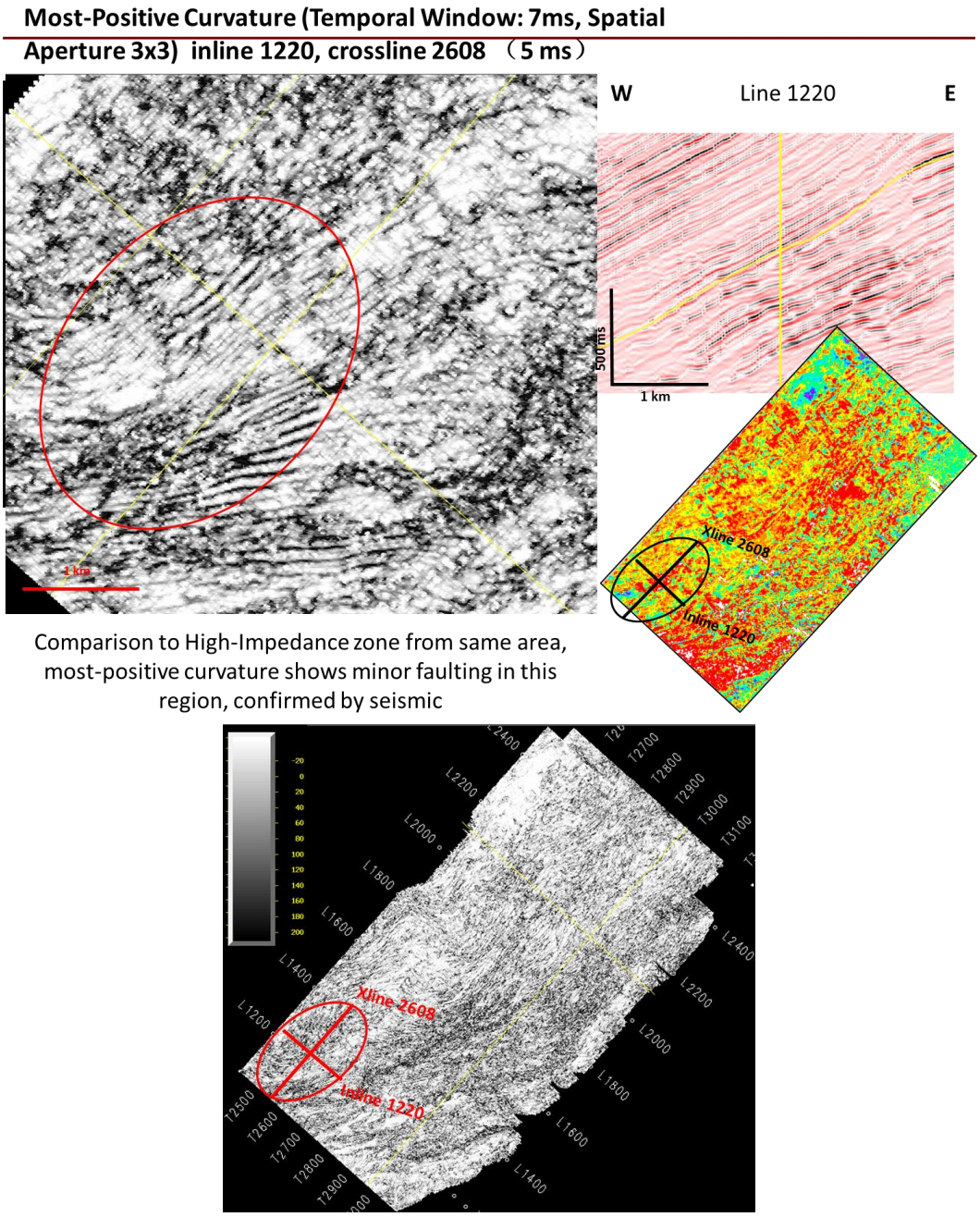

Figure 4.19 – Comparison of impedance and curvature horizon slices at 5ms, where a low-impedance zone is observed in the southwest. Interpretation from high-resolution dataset and most-positive curvature horizon confirms that there exists evidence of minor faults in the zone.

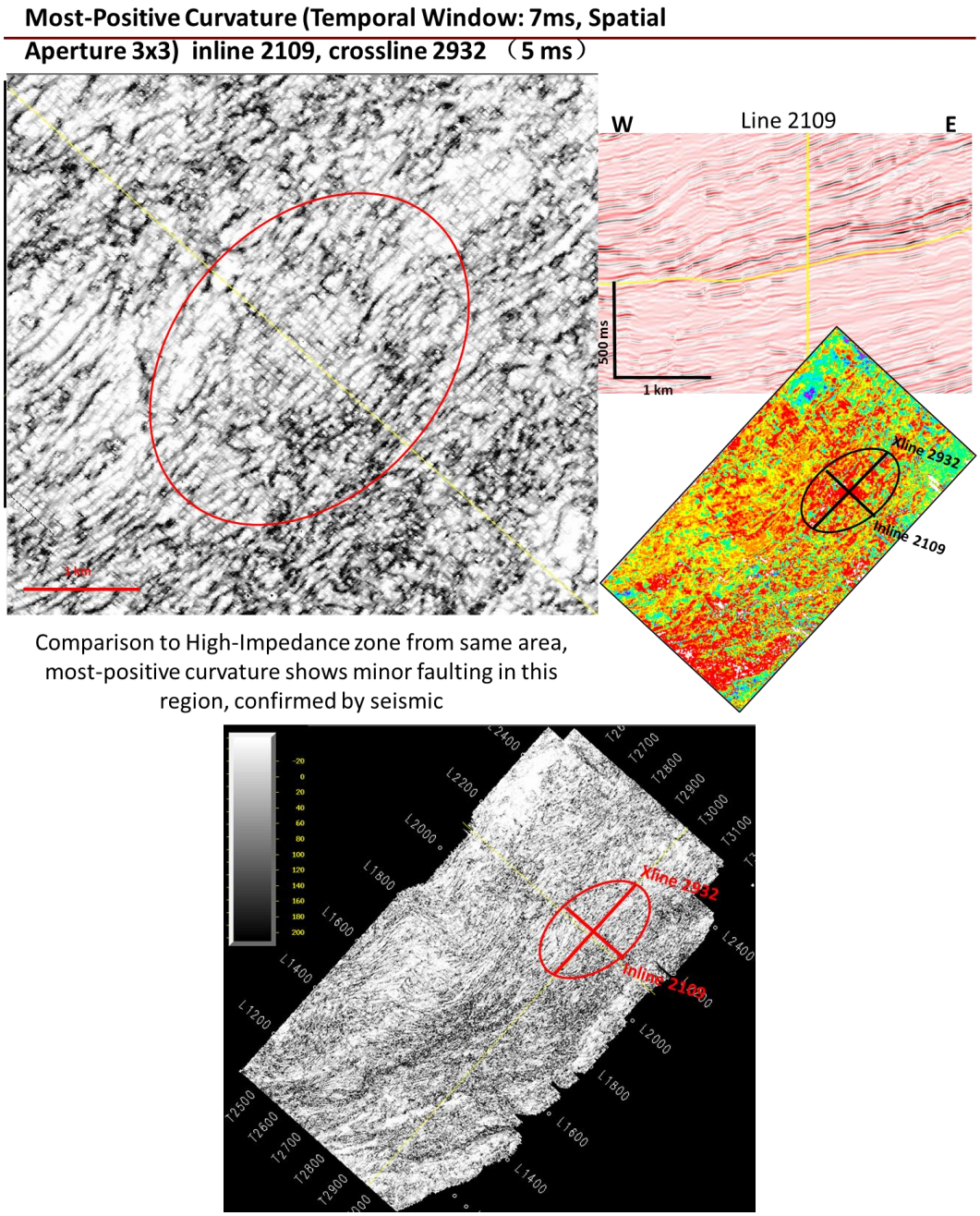

Figure 4.20 – Comparison of impedance and curvature horizon slices at 5ms, where a low-impedance zone is observed in the northeast. Interpretation from high-resolution dataset and most-positive curvature horizon confirms that there exists evidence of minor faults in the zone.

Conclusions

We find that for the high-resolution volume, the 8-trace eigenstructure coherence analysis is still the optimal method of describing the general and large-scale faulting in the dataset. Likewise, most-positive curvature best describes the smaller faulting and possible fracture networks in the high resolution volume as well. These two attribute analyses used together provide the interpreter with tools for mapping the regional faults and identifying the minor faults and fractures which may result from those large-fault networks, and when confirmed by interpretation to seismic data, become a powerful reservoir characterization tool.

For prospecting and reservoir planning in the future of the Huabei Field, we focus on the most-positive curvature along the Reservoir Top horizon and below, describing the minor faulting and matching those areas to low impedance zones. We observe evidence of faulting and possible fracturing in each of these low-impedance areas, which identifies these zones and depths within the reservoir as potential prospects, due to the nature of fractures in carbonates and the presence of shows in exploratory wells in the area.

CHAPTER V

CONCLUSIONS

From the results of our investigation, we are able to obtain a good representation of the fracture network in a North China field from both low and high resolution seismic volumes using coherency, curvature, and seismic volumes for interpretation. We have also identified the optimal attribute analyses methods and parameters to use for describing large and small-scale faulting in the carbonate reservoir for the low and high-resolution data. We find that most-positive curvature is the most effective seismic attribute analysis for describing small faults and predicting fracture density in the Huabei dataset, especially near the highly-faulted zones through the carbonate reservoir.

The results of this research can contribute to the understanding and prediction of fracture networks resulting from faulting and diagenesis in carbonate reservoirs. The methodology applied for major and minor fault mapping are applicable, or at least adaptable, to other carbonate fields with similarly identifiable fault networks. Furthermore, the experimentally established relationship between measured values from acquired data (coherency, curvature) to impedance inversion from well data and possible connection to production data (fracture density) can be applied in future exploration and prospecting practices in similar carbonate fields. Understanding and accurately mapping the fracture networks which result from faults and diagenesis in carbonate reservoirs assists petroleum companies in reservoir characterization and increases the confidence in prospect determination in fields of interest. Favorable trapping can be identified, fracture-driven efficiencies in hydrocarbon extraction can be exploited, less investment is needed in

exploratory wells, and we can increase recovery of hydrocarbons from complex, carbonate fields.

The next steps to continue the investigation would be to sample the impedance and curvature horizon slices at a smaller interval over a longer period of time (depth) to fully characterize the carbonate reservoir through the field using these two attribute analyses. Doing so would help clarify the dimensional extents of minor fault/fracture density within the prospects to classify them by potential reservoir volume and quality. This could lead to carbonate reservoir modeling and the initial steps to perhaps establishing an empirical relationship between seismic attributes and petrophysical properties.

REFERENCES

Al-Dossary, S., and K. J. Marfurt, 2006, Multispectral estimates of reflector curvature and rotation: Geophysics, **71**, 41-51.

Al-Dossary, S., and K. J. Marfurt, 2003, Improved 3-D seismic edge detection filter applied to Vinton Dome, Louisiana: 73rd Annual International Meeting, SEG, Expanded Abstracts, 2370-2372

Bahorich, M. S., and S. L. Farmer, 1995, 3-D seismic discontinuity for faults and stratigraphic features: The coherence cube, The Leading Edge, **14**, 1053-1058.

Bahorich, M. S., J. A. Lopez, N. L. Haskell, S. E. Nissen, and A. Poole, 1995, Stratigraphic and structural interpretation with 3-D coherence: 65th Annual International Meeting, SEG, Expanded Abstracts, 97-100.

Brown, A. R., and J. D. Robertson, 1985, Focusing on SEG continuing education - Seismic interpretation for detailed exploration development and production: The Leading Edge, **4**, 60-65.

Bednar, J. B., 1998, Least-squares dip and coherency attributes: The Leading Edge, **17**, 775-776.

Briggs I.C., 1974. Machine contouring using minimum curvature, Geophysics, **39**, 39–48.

Clumentritt, C. H., E. C. Sullivan, and K. J. Marfurt, 2003, Channel detection using seismic attributes on the Central Basin Platform, West Texas: 73rd Annual International Meeting, SEG, Expanded Abstracts, 466-469.

Chopra, S., 2002, Coherence cube and beyond: First Break, **20**, no. 01, 27-33.

Chopra, S., V. Alexeev, and Y. Xu, 2003, 3D AVO cross-plotting - An effective visualization technique: The Leading Edge, **22**, 1078-1089.

Chopra, S., and K. J. Marfurt, 2005, Seismic attributes - A historical perspective: Geophysics, **70**, 3SO-28SO.

Chopra, S., and K. J. Marfurt, 2007a, Seismic Attributes for Prospect Identification and Reservoir Characterization, SEG.

Chopra, S., and K. J. Marfurt, 2007b, Seismic attributes for fault/fracture characterization: 77th Annual International Meeting, SEG, Expanded Abstracts, 1520-1524.

Chopra, S., and K. J. Marfurt, 2007c, Volumetric curvature-attribute applications for

detection of fracture lineaments and their calibration: Geohorizons, 27-31.

Chopra, S., and K. J. Marfurt, 2007d, Multispectral volumetric curvature adding value to 3D seismic data interpretation: CSPG/CSEG Convention, Calgary.

Ericsson, J. B., H. C. McKeon, and R. J. Hooper, 1988, Facies and curvature controlled 3-D fracture models in a Cretaceous carbonate reservoir, Arabian Gulf: Geological Society of London Special Publication 147, 299-312.

Han, Tianbao, Cheng, Peng, Wang, Yongli, Zhang Jindong, Fang, Haifei, A method of predicting carbonate reservoir heterogeneity - a case study of carbonate reservoir in Hexiwu, Huabei: OGP, 2011, 46(1), 102-105.

Hart, B.S., 2002, Validating seismic attributes: Beyond statistics, The Leading Edge, **21**, 1016-1021.

Kalkomey, C. T., 1997, Potential risks when using seismic attributes as predictors of reservoir properties: The Leading Edge, **16**, 247-251.

Lisle, R. J., 1994, Detection of zones of abnormal strains in structures using Gaussian curvature analysis: AAPG Bulletin, **78**, 1811-1819.

Marfurt, K. J., 2006, Robust estimates of 3D reflector dip and azimuth: Geophysics, **71**, 29-40.

Marfurt, K. J., R. L. Kirlin, S. H. Farmer, and M. S. Bahorich, 1998, 3-D seismic attributes using a running window semblance-based algorithm: Geophysics, **63**, 1150-1165.

Marfurt, K. J., and R. L. Kirlin, 2000, 3-D broad-band estimates of reflector dip and amplitude: Geophysics, **65**, 304–320.

Marfurt, K. J., V. Sudhakar, A. Gersztenkorn, K. D. Crawford, and S. E. Nissen, 1999, Coherency calculations in the presence of structural dip: Geophysics, **64**, 104-111.

Masaferro, J. L., M. Bulnes, J. Poblet, and M. Casson, 2003, Kinematic evolution and fracture prediction of the Valle Morado structure inferred from 3-D seismic data, Salta Province, northwest Argentina, American Association of Petroleum Geologists Bulletin, **87**, 1083-1104.

Nissen, S. E., T. R. Carr, K. J. Marfurt, and E. C. Sullivan, 2009, Using 3D seismic volumetric curvature attributes to identify fracture trends in a depleted Mississippian carbonate reservoir: Implications for assessing candidates for CO2 sequestration: AAPG Studies in Geology, **59**, 297–319.

Roberts, A., 2001, Curvature attributes and their application to 3-D interpreted horizons: First Break, **19**, 85-99.

Sigismondi, E. M., and C.J. Soldo, 2003, Curvature attributes and seismic interpretation: Case studies from Argentina basins: The Leading Edge, **22**, 1122-1126.

Zha, Quanheng, 1984, Jizhong Depression, China - Its geologic framework, evolutionary history, and distribution of hydrocarbons: The American Association of Petroleum Geologists Bulletin, **68**, 983-992.

Zhang, T., Li, A., Sun, Y., Tian, J., Lu, L., Zhang, R., and Zhao, X., High-resolution characterization of fractured carbonate reservoirs integrating seismic inversion and attributes analysis, Bohai Bay Basin, China. Part I: Rock physics analysis and post-stack seismic inversion. To be submitted to Journal of Applied Geophysics.